Aerospace Science and Technology 146 (2024) 108945

Contents lists available at ScienceDirect

Aerospace Science and Technology

journal homepage: www.elsevier.com/locate/aescte

Free-floating space manipulator impacting a floating object: Modeling and output SDRE controller design

Saeed Rafee Nekoo [a,*], Inna Sharf [b], Anibal Ollero [a,c]

[a] The GRVC Robotics Lab., Departamento de Ingeniería de Sistemas y Automática, Escuela Técnica Superior de Ingeniería, Universidad de Sevilla, Seville, 41092, Spain
[b] Department of Mechanical Engineering, McGill University, Montreal, Quebec, H3A 0C3, Canada
[c] FADA-CATEC, Centro Avanzado de Tecnologías Aeroespaciales, Seville, 41300, Spain

ARTICLE INFO

Communicated by Christian Circi

Keywords:
Free-floating space manipulator
Space robotics
SDRE
OSDRE
Output feedback control
Linear and angular momentum

ABSTRACT

This work investigates the dynamics modeling, control, and impact resolution between a floating object and a free-floating space manipulator (FFSM). The controller design is carried out by using an output- and state-dependent Riccati equation (OSDRE) approach. In a collision between an object and a mechanism, the computation of the generalized velocities and the impact force or impulse, which are interrelated, is a challenging problem. Taking into account the free-floating conditions of the space environment, the conservation of linear and angular momentum equations, combined with the conservation of kinetic energy under the elastic impact assumption, are used to find the unknown variables of the impact problem. The control problem addressed for the FFSM is to regulate its end-effector in a point-to-point motion scenario, this while the space manipulator suffers an unintended impact with a floating object, such as a damaged satellite or space debris. By proposing a safety pause starting with the occurrence of impact and for a short duration thereafter, the proposed OSDRE design succeeds in achieving the end-effector regulation control. Although the FFSM can reach the target point, it is shown that maintaining the end-effector regulation at the target is not feasible due to the momentum imparted to the FFSM as a result of the collision. To this end, we employ a simple thruster control on the space manipulator base to complete the regulation task. The theoretical development and controller design are demonstrated through a simulation case study of a spacecraft equipped with a three-link manipulator colliding with an object.

1. Introduction

The number of satellites, space debris, and floating objects orbiting around Earth is increasing rapidly due to technological progress and growth of the space industry. This points to the necessity to study the interaction of space manipulators with floating objects. The purpose of the interaction can be on-orbit repair [1,2], maintenance [3,4], collection of debris [5] and grasping of debris [6]; however, a very likely occurrence in space operations is an unintended collision between a space manipulator and a floating object. The ideal scenario in such a situation would be the completion of a control task by the space manipulator, even though it suffered a collision. In this paper, we focus on a free-floating space manipulator (FFSM) which includes a robotic arm, mounted on a floating base when the thrusters of the base are turned off [7,8]. Using the floating characteristics of the FFSM, the dynamics of the mounted arm can be presented in a compact form including the state variables of the base. To resolve the impact resulting from the collision, for both the floating object and the FFSM, we employ the appropriate momentum conservation equations to define relationships between the velocities of the components of the colliding system before and after impact. An additional equation used to complete the resolution of impact is the conservation of energy over the impact, which applies to elastic frictionless impacts between the gripper and the floating object. Thus, the principal assumptions for this work are a floating condition for both the FFSM and the colliding object, elastic and frictionless impact, and hence, no energy dissipation over the impact.

The study of impact in robotic and, more generally, multibody systems has a long and rich history in the scientific community [9–11]. The Jacobian matrix and force control are two useful tools for analyzing and controlling a manipulator interacting with the environment [12,13]. This approach is helpful since the contact point of the gripper and the base of the robotic arm are fixed. Rhee et al. presented hybrid

* Corresponding author.
E-mail addresses: saerafnek@us.es, saerafee@yahoo.com (S.R. Nekoo).

https://doi.org/10.1016/j.ast.2024.108945
Received 3 November 2023; Received in revised form 1 January 2024; Accepted 29 January 2024
Available online 1 February 2024

admittance and impedance control for impact scenarios of robotic manipulators [14]. Jung et al. used robust variable structure control for position and force control of the arm in contact with the environment [15]. The extension of the topic leads to capturing an object or payload with space manipulators [16].

A challenge in the collision between a mechanism and an object is the computation of the impact force and post-impact velocities. Dimitrov and Yoshida used a biased momentum approach to find the distribution of the momentum in a manipulator to analyze the post-impact phase [17]. Capturing objects in space includes impact in the formulation. Nagaoka et al. used a repeated impact-based capturing method for a tumbling object in space by a dual-arm manipulator [18]. Passive damping was proposed to solve the impact issue in the control task. Liu et al. designed a new end-effector for refueling satellites which included the impact modeling and contact analysis for space missions [19]; the end-effector was designed to perform docking and refueling tasks with a single arm instead of a dual-arm system. Modeling the object capture as inelastic impact allows us to simply "add" the object to the end-effector and is a common approach to address the problem of object capture in space. Raina et al. proposed reaction-less control for a post-impact phase in capturing objects by using the inelastic impact assumption in dynamics modeling and control [20]. A dual-arm servicing robot was simulated capturing an object.

Research on bipedal humanoid robots provides numerous examples of solving the impact dynamics and control problem involving complex multi-link mechanisms [21,22]. The oblique impact was proposed for a multi-link system in contact with the environment [22]. It was shown that the equation of motion for the system could be integrated over the impact to obtain an algebraic equation involving the inertia matrix and the difference between the velocities of the joints before and after the collision. Nekomoto and Sekiguchi modeled and controlled a biped system and analyzed the impact [23]. The difference between the impact of bipeds with the ground and the impact that occurs between objects in space is the absence of gravity and the floating condition [24,25]. The analysis of the impact force and integration of the equation of motion can be adopted for impact in space, where similarly the Coriolis and centrifugal terms vanish [26,27] when integrated over impact. The advantage of impact analysis for biped locomotion is the possibility of experimentation with real systems [28,29].

The state-dependent Riccati equation (SDRE) is chosen here to control an FFSM in a regulation task. This controller possesses a sub-optimal design and includes nonlinearity of the dynamics of the system in its structure [30]. The capability of the controller to balance the precision of the state convergence and input efforts through the cost function integral of the SDRE is a great benefit for easy tuning of the controller [31,32]. The use of the SDRE approach in space and satellite applications began in the late 90s when the SDRE was proposed for satellite attitude control [33]. Space applications of the SDRE control include satellites/spacecraft [34,35], docking [36], CubeSats [37], and space robotics [38]. In this work, the focus is on applying the SDRE controller to space robotics, specifically for post-impact regulation of an FFSM.

Space manipulators or space robotic arms, which subsume a single manipulator, dual-arm systems, or multiple arms, are popular systems for operations involving interaction with objects, satellites, or space debris. They are usually intended to operate either in free-floating (without the actuation of the base) or free-flying (with the actuation of the base) modes, while the manipulator system is in operation. Sharma and Rout presented a reaction-less multi-arm space manipulator for cooperative tasks [39]. The proposed application was construction in space and manipulation; the multi-arm design was carried out to perform energy-efficient manipulation. Typically, the mass of the base of the space manipulator, particularly for the free-floating systems, is relatively large so that it naturally compensates for the reactions imparted by the motion of the arm [40]. The mass difference between the base and the arm is justified since the base carries a power supply, sensors, fuel, and other required hardware and components. The model-reference SDRE was designed in [40] and compared in simulation for light vs. heavy-base systems, to evaluate the theoretical feasibility of controller performance without increasing the actual mass of the base. An et al. researched in-orbit assembly and construction by using dual-arm FFSM via convex programming [41]. Convex programming was used to perform time-optimal path tracking.

An ideal controller for an FFSM considers the deviation of the FFSM's base in the point-to-point maneuvers. The output- and state-dependent Riccati equation (OSDRE) derivation is based on the output feedback control method, applied on the sub-optimal control SDRE [42]. Using OSDRE, the mass of the base could be reduced to the same order of magnitude as the mass of the arm. Another advantage of the OSDRE is more precision in regulating the gripper in a control task. Since the objective is to guide the gripper to the final point, the base and the torque of the arms work to achieve the task, and the perturbation of the base does not affect the success rate of the control. However, for the model-reference SDRE design, the controller was sensitive to perturbation of the base and its deviations caused more errors in the end-effector regulation [40]. The impact dynamics and the SDRE control in the robotics field were studied quite recently [43] where the authors presented force and impact control for a fixed-base robotic manipulator in contact with the environment. The impact of space robotic manipulators using OSDRE controller design is addressed here. This work aims to complete a regulation control task, when an unintended collision occurs in the middle of the trajectory, as may occur, for example, when a collision avoidance strategy fails. Therefore, in this work, we study the system modeling over impact, for both the FFSM and the object, and address the control problem with consideration of the impact, which has not been studied in the SDRE domain.

The main contributions of this paper are:

C1. Impact modeling and resolution in space for a complex mechanism (FFSM) colliding with a floating object.
C2. A general method to compute the generalized velocities of the FFSM involved in elastic impact by using conservation of momentum and conservation of energy equations.
C3. Formulation and implementation of the OSDRE regulation control for an FFSM undergoing collision during a point-to-point task.

Notation: $(\cdot)^\top$ denotes the transpose of a vector or a matrix, $\delta(\cdot)$ shows impulse, $\mathbb{R}^n$ indicates n-dimensional Euclidean space, $(\cdot)^\dagger$ is the generalized inverse of a vector or a matrix, $\mathbb{R}^{n\times m}$ shows an $n \times m$ real matrix, $\mathbf{0}_{n\times n}$ and $\mathbf{I}_{n\times n}$ denote zero and identity matrices of size $n \times n$, respectively, and $\mathrm{diag}(\cdot)$ denotes a matrix with diagonal components.

Structure of the paper: Section 2 presents the dynamics modeling of the floating object, FFSM, and the impact resolution. The OSDRE control formulation is summarized in Section 3. It also includes the statement of necessary conditions for implementing the control for the FFSM, considering the impact. Section 4 demonstrates the performance of OSDRE through a simulation study of an FFSM with a three-degree-of-freedom (DoF) arm, undergoing a planar collision with an object, with accompanying discussion of the system responses, both pre- and post-impact. Particular attention is given to the validation of the results by providing momenta and energy responses. The final remarks are stated in Section 5.

2. Modeling: mathematical representation of dynamics

The mathematical model of the system is presented in this section, including the dynamics equation of the floating object, the equation of motion of the FFSM, and the impact modeling. The schematic of the FFSM moving from the initial to the final condition is shown in Fig. 1. We assume that a floating object (e.g., an out-of-service satellite, a CubeSat, space debris) is on the path of the end-effector of the arm and a collision happens. The objective is to model the impact phase

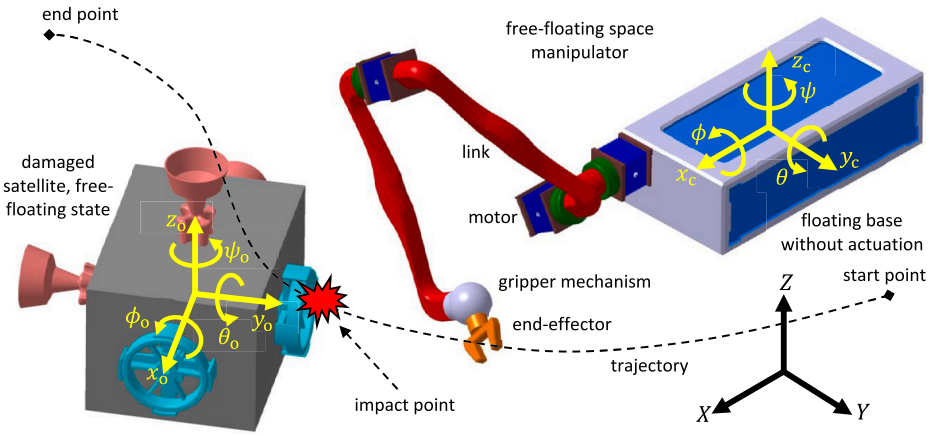

Fig. 1. The inertial and body-fixed frame definition, a schematic of the free-floating space manipulator and floating object (in this case a floating damaged satellite or an out-of-fuel CubeSat), and end-effector trajectory with possible impact. $\phi_o(t), \theta_o(t), \psi_o(t)$ show base orientation of the floating object and $\phi(t), \theta(t), \psi(t)$ show base orientation of the FFSM w.r.t. global reference $\{X, Y, Z\}$.

and to simulate the ensuing motions of both the object and the FFSM after the impact. We assume that at the moment of impact, a safety switch turns off the actuators of the space manipulator to avoid further damage. Following a pre-defined duration security pause, the manipulator regulates the gripper toward the final desired condition in the point-to-point control task.

As was alluded in the introduction, obstacle avoidance methods are indeed well-developed in literature, including methods such as artificial potential field [44–46], the SDRE obstacle avoidance [47–49], the rapidly exploring random tree algorithm [50,51] and others. However, the goal of this work is to model the collision in space in the context of the regulation task of the FFSM, and the collision is intentionally designed to study this topic.

Assumption 1. Perturbations such as atmospheric drag, solar radiation pressure, and other external disturbances are considered to be negligible w.r.t. the forces of the FFSM while operating in space.

Assumption 2. Orbital mechanics is neglected and it is assumed that the local orbital frame is the inertial, also referred to as the global frame.

2.1. Dynamics model of the floating object

The generalized coordinates of the floating object are collected into a column vector $\mathbf{q}_o(t) = [x_o(t), y_o(t), z_o(t), \phi_o(t), \theta_o(t), \psi_o(t)]^\top$, where the position is defined by $\boldsymbol{\xi}_{o,1}(t) = [x_o(t), y_o(t), z_o(t)]^\top$, and the orientation is parameterized by $\boldsymbol{\xi}_{o,2}(t) = [\phi_o(t), \theta_o(t), \psi_o(t)]^\top$, w.r.t. to the inertial reference frame. The state variables of the floating object are arranged into

$$\mathbf{x}_o(t) = \begin{bmatrix} \boldsymbol{\xi}_{o,1}(t) \\ \boldsymbol{\xi}_{o,2}(t) \\ \dot{\boldsymbol{\xi}}_{o,1}(t) \\ \dot{\boldsymbol{\xi}}_{o,2}(t) \end{bmatrix}, \tag{1}$$

where the following relationships hold between the generalized velocities and the body-fixed linear ($\boldsymbol{\upsilon}_{o,1}(t)$) and angular ($\boldsymbol{\upsilon}_{o,2}(t)$) velocities of the object:

$$\begin{aligned} \dot{\boldsymbol{\xi}}_{o,1}(t) &= \mathbf{R}(\boldsymbol{\xi}_{o,2}(t))\boldsymbol{\upsilon}_{o,1}(t), \\ \dot{\boldsymbol{\xi}}_{o,2}(t) &= \mathbf{T}(\boldsymbol{\xi}_{o,2}(t))\boldsymbol{\upsilon}_{o,2}(t), \end{aligned} \tag{2}$$

in which

$$\mathbf{R}(\boldsymbol{\xi}_{o,2}(t)) = \begin{bmatrix} c_{\psi_o}c_{\theta_o} & -c_{\phi_o}s_{\psi_o} + s_{\phi_o}s_{\theta_o}c_{\psi_o} & s_{\phi_o}s_{\psi_o} + c_{\phi_o}s_{\theta_o}c_{\psi_o} \\ s_{\psi_o}c_{\theta_o} & c_{\phi_o}c_{\psi_o} + s_{\phi_o}s_{\theta_o}s_{\psi_o} & -s_{\phi_o}c_{\psi_o} + c_{\phi_o}s_{\theta_o}s_{\psi_o} \\ -s_{\theta_o} & c_{\theta_o}s_{\phi_o} & c_{\theta_o}c_{\phi_o} \end{bmatrix},$$

$$\mathbf{T}(\boldsymbol{\xi}_{o,2}(t)) = \begin{bmatrix} 1 & s_{\phi_o}t_{\theta_o} & c_{\phi_o}t_{\theta_o} \\ 0 & c_{\phi_o} & -s_{\phi_o} \\ 0 & s_{\phi_o}/c_{\theta_o} & c_{\phi_o}/c_{\theta_o} \end{bmatrix}.$$

The translational and orientation dynamics equations of the floating object can be obtained by employing the Lagrangian formulation to give:

$$m_o\ddot{\boldsymbol{\xi}}_{o,1}(t) = \mathbf{F}_e\delta(t - t_i), \tag{3}$$

$$\mathbf{I}(\boldsymbol{\xi}_{o,2}(t))\ddot{\boldsymbol{\xi}}_{o,2}(t) + \mathbf{C}(\boldsymbol{\xi}_{o,2}(t), \dot{\boldsymbol{\xi}}_{o,2}(t))\dot{\boldsymbol{\xi}}_{o,2}(t) = \boldsymbol{\tau}_e\delta(t - t_i), \tag{4}$$

where m_o is the mass of the object, $\mathbf{F}_e \in \mathbb{R}^3$ represents the impulsive external force due to the impact, expressed in global coordinates $\{XYZ\}$, $\delta(t - t_i)$ is the Dirac delta function, t_i is the time of impact, $\mathbf{I}(\boldsymbol{\xi}_{o,2}(t)) = \mathbf{T}^{-\top}(\boldsymbol{\xi}_{o,2}(t))\mathbf{I}_c\mathbf{T}^{-1}(\boldsymbol{\xi}_{o,2}(t))$ is the generalized inertia of the object corresponding to the orientation coordinates $\boldsymbol{\xi}_{o,2}(t)$, in which $\mathbf{I}_c = \mathrm{diag}(I_{xx}, I_{yy}, I_{zz})$ is the centroidal principal-axes inertia matrix of the floating object. The term

$$\mathbf{C}(\boldsymbol{\xi}_{o,2}(t), \dot{\boldsymbol{\xi}}_{o,2}(t))\dot{\boldsymbol{\xi}}_{o,2}(t) : \mathbb{R}^3 \times \mathbb{R}^3 \to \mathbb{R}^3,$$

models the Coriolis and centrifugal effects. The column vector $\boldsymbol{\tau}_e \in \mathbb{R}^3$ contains the generalized impulsive torque about the CoM of the floating object resulting from the impact force.

The time derivative of the state-vector (1) with the substitution of (3)-(4) results in the state-space (SS) model of the object:

$$\dot{\mathbf{x}}_o(t) = \begin{bmatrix} \dot{\boldsymbol{\xi}}_{o,1}(t) \\ \dot{\boldsymbol{\xi}}_{o,2}(t) \\ \frac{1}{m_o}\mathbf{F}_e\delta(t - t_i) \\ \mathbf{I}^{-1}(\boldsymbol{\xi}_{o,2}(t))[\boldsymbol{\tau}_e\delta(t - t_i) - \mathbf{C}(\boldsymbol{\xi}_{o,2}(t), \dot{\boldsymbol{\xi}}_{o,2}(t))\dot{\boldsymbol{\xi}}_{o,2}(t)] \end{bmatrix}. \tag{5}$$

Prior to impact, there are no external forces or moments applied to the object and it is assumed that the object is initially stationary and non-rotating. The impact creates an impulsive input on the object and its subsequent motion as per (5) depends on the point of impact, as well as the direction and magnitude of the impulsive force. Following the impact, the external force vanishes again and the floating object reacts to the impulse freely.

With the view to employing the discrete model of impact between the object and the FFSM [9], we introduce the linear momentum $\mathcal{P}_o$ and the angular momentum $\mathcal{L}_o$ of the object, the latter about the origin of the inertial (global) frame $\{X, Y, Z\}$. The two momenta can be compactly formulated as:

$$\begin{bmatrix}\mathcal{P}_{\mathrm{o}}\\ \mathcal{L}_{\mathrm{o}}\end{bmatrix}=\begin{bmatrix}m_{\mathrm{o}}\dot{\boldsymbol{\xi}}_{\mathrm{o},1}(t)\\ \mathbf{R}(\boldsymbol{\xi}_{\mathrm{o},2}(t))[\mathbf{I}_{\mathrm{c}}\boldsymbol{\upsilon}_{\mathrm{o},2}(t)]+\boldsymbol{\xi}_{\mathrm{o},1}(t)\times m_{\mathrm{o}}\dot{\boldsymbol{\xi}}_{\mathrm{o},1}(t)\end{bmatrix},\tag{6}$$

where we point out the second term in the expression for $\mathcal{L}_{\mathrm{o}}$, which represents the moment of the linear momentum about the inertial origin. Both momenta are initially zero and are conserved until impact occurs. At the instant of collision, the two momenta experience a discontinuous change, and once again remain conserved at their new values thereafter. It is also worth noting that prior to and after impact, the angular momentum of the object about its center of mass, represented by the first term in the expression for $\mathcal{L}_{\mathrm{o}}$, is also conserved. However, since the collision takes place with a multibody system—the FFSM—and in anticipation of impact resolution for the object-FFSM system, the angular momentum of the object about the origin of the inertial frame will be required, as per the definition in (6).

2.2. Dynamics model of FFSM

The generalized coordinates of the FFSM system are combined into:

$$\mathbf{q}(t)=[\mathbf{q}_{\mathrm{b}}^{\top}(t),\mathbf{q}_{\mathrm{a}}^{\top}(t)]^{\top},$$

where $\mathbf{q}_{\mathrm{b}}(t)=[x_{\mathrm{c}}(t),y_{\mathrm{c}}(t),z_{\mathrm{c}}(t),\phi(t),\theta(t),\psi(t)]^{\top}$ contains the generalized coordinates of the base, with the CoM position of the floating base represented by $\boldsymbol{\xi}_1(t)=[x_{\mathrm{c}}(t),y_{\mathrm{c}}(t),z_{\mathrm{c}}(t)]^{\top}$ and the orientation of the base parameterized by $(\phi(t),\theta(t),\psi(t))$ in the global reference $\{X,Y,Z\}$. The generalized coordinates of the arm are:

$$\mathbf{q}_{\mathrm{a}}(t)=\begin{bmatrix}q_1(t)\\ \vdots\\ q_N(t)\end{bmatrix},$$

where N is the number of joints or DoF of the manipulator. The dynamics equation of the FFSM subject to a reactive impact force as a result of a collision with the floating object at time t_{i} can be stated as [42]:

$$\begin{bmatrix}\mathbf{M}_{\mathrm{b}}(\mathbf{q}(t)) & \mathbf{M}_{\mathrm{b,a}}(\mathbf{q}(t))\\ \mathbf{M}_{\mathrm{b,a}}^{\top}(\mathbf{q}(t)) & \mathbf{M}_{\mathrm{a}}(\mathbf{q}(t))\end{bmatrix}\begin{bmatrix}\ddot{\mathbf{q}}_{\mathrm{b}}(t)\\ \ddot{\mathbf{q}}_{\mathrm{a}}(t)\end{bmatrix}+\begin{bmatrix}\mathbf{c}_{\mathrm{b}}(\mathbf{q}(t),\dot{\mathbf{q}}(t))\\ \mathbf{c}_{\mathrm{a}}(\mathbf{q}(t),\dot{\mathbf{q}}(t))\end{bmatrix}=\begin{bmatrix}\mathbf{0}\\ \mathbf{u}(t)\end{bmatrix}-\mathbf{J}^{\top}(\mathbf{q}(t))\mathbf{F}_{\mathrm{e}}\delta(t-t_{\mathrm{i}}),\tag{7}$$

where the base inertia matrix is $\mathbf{M}_{\mathrm{b}}(\mathbf{q}(t)):\mathbb{R}^{6+N}\to\mathbb{R}^{6\times 6}$, the interaction of the inertia between the arm and base is $\mathbf{M}_{\mathrm{b,a}}(\mathbf{q}(t)):\mathbb{R}^{6+N}\to\mathbb{R}^{6\times N}$, the arm inertia matrix is $\mathbf{M}_{\mathrm{a}}(\mathbf{q}(t)):\mathbb{R}^{6+N}\to\mathbb{R}^{N\times N}$, the Coriolis and centrifugal components of the base are collected in $\mathbf{c}_{\mathrm{b}}(\mathbf{q}(t),\dot{\mathbf{q}}(t)):\mathbb{R}^{6+N}\times\mathbb{R}^{6+N}\to\mathbb{R}^{6}$, those for the arm are denoted as $\mathbf{c}_{\mathrm{a}}(\mathbf{q}(t),\dot{\mathbf{q}}(t)):\mathbb{R}^{6+N}\times\mathbb{R}^{6+N}\to\mathbb{R}^{N}$, and $\mathbf{J}(\mathbf{q}(t)):\mathbb{R}^{6+N}\to\mathbb{R}^{3\times(6+N)}$ is the Jacobian matrix of the FFSM. Finally, the input forces and/or torques of the motors of the manipulator are collected in the input column vector $\mathbf{u}(t)\in\mathbb{R}^{N}$.

Remark 1. The sign in front of the impact force term in (7) is negative to reflect the fact that it is a reaction of the impulsive force applied to the object, as per the object dynamics in (3).

Remark 2. Under the free-floating conditions that exist for FFSM before and after impact, the total linear momentum and the total angular momentum of FFSM, the latter about the origin of the inertial frame, are each conserved. As a result of the impact, additional linear and angular momenta are imparted to FFSM; therefore, these, with the angular momentum about the origin of the inertial frame, will be conserved at their post-impact values, as per impact resolution.

The integration of the upper set of the equation of motion (7) results in:

$$\begin{bmatrix}\mathcal{P}_{\mathrm{FFSM}}\\ \mathcal{L}_{\mathrm{FFSM}}\end{bmatrix}=\mathbf{M}_{\mathrm{b}}(\mathbf{q}(t))\dot{\mathbf{q}}_{\mathrm{b}}(t)+\mathbf{M}_{\mathrm{b,a}}(\mathbf{q}(t))\dot{\mathbf{q}}_{\mathrm{a}}(t),\tag{8}$$

in which $\mathcal{P}_{\mathrm{FFSM}}\in\mathbb{R}^3$ and $\mathcal{L}_{\mathrm{FFSM}}\in\mathbb{R}^3$ are the system's linear and angular momenta of the FFSM. It is noted that the angular momentum of the FFSM computed from the system inertia matrices in (8) is about the CoM of the base of the FFSM. This angular momentum becomes equivalent to the angular momentum about the origin of the inertial frame only when the linear momentum of the system is zero.

Under the assumptions made in this paper, that the FFSM is initially stationary and in light of the comments above, we can claim conservation of both momenta in (8) during the pre-impact motion of the FFSM system. After impact, the linear momentum of the FFSM is no longer zero, and therefore, its angular momentum about the CoM of the base, i.e., $\mathcal{L}_{\mathrm{FFSM}}$ in equation (8), is not conserved, but changes with time. However, the angular momentum of the FFSM about inertial frame origin is conserved and it can be computed from the momenta in (8) as $\mathcal{L}_{\mathrm{FFSM}}+\boldsymbol{\xi}_1(t)\times\mathcal{P}_{\mathrm{FFSM}}$. For later use, we re-state the linear momentum and the angular momentum of the FFSM about the origin of the inertial frame in compact form as:

$$\begin{bmatrix}\mathcal{P}_{\mathrm{FFSM}}\\ \mathcal{L}_{\mathrm{FFSM,I}}\end{bmatrix}=\begin{bmatrix}\mathcal{P}_{\mathrm{FFSM}}\\ \mathcal{L}_{\mathrm{FFSM}}+\boldsymbol{\xi}_1(t)\times\mathcal{P}_{\mathrm{FFSM}}\end{bmatrix},\tag{9}$$

where subscript"I" denotes the angular momentum computation about the origin of the inertial frame.

2.3. Impact modeling

2.3.1. Post-impact velocity computation

In the mathematical modeling of the floating object in Section 2.1 and the FFSM system in Section 2.2, the external input force and torque are impulsive and are applied at a specific instance of time. Two sets of values associated with impact must be computed: the change in the velocity of the states, for both the object and the FFSM, and also the impulse created by the impact force. As noted earlier, at the moment of impact the actuators of the FFSM are turned off ($\mathbf{u}(t)=\mathbf{0}$), so that the equations of motion for the FFSM (7) simplify to:

$$\mathbf{M}(\mathbf{q}(t))\ddot{\mathbf{q}}(t)+\mathbf{c}(\mathbf{q}(t),\dot{\mathbf{q}}(t))=-\mathbf{J}^{\top}(\mathbf{q}(t))\mathbf{F}_{\mathrm{e}}\delta(t-t_{\mathrm{i}}),\tag{10}$$

in which the FFSM system matrices are introduced:

$$\mathbf{M}(\mathbf{q}(t))=\begin{bmatrix}\mathbf{M}_{\mathrm{b}}(\mathbf{q}(t)) & \mathbf{M}_{\mathrm{b,a}}(\mathbf{q}(t))\\ \mathbf{M}_{\mathrm{b,a}}^{\top}(\mathbf{q}(t)) & \mathbf{M}_{\mathrm{a}}(\mathbf{q}(t))\end{bmatrix},$$

$$\mathbf{c}(\mathbf{q}(t),\dot{\mathbf{q}}(t))=\begin{bmatrix}\mathbf{c}_{\mathrm{b}}(\mathbf{q}(t),\dot{\mathbf{q}}(t))\\ \mathbf{c}_{\mathrm{a}}(\mathbf{q}(t),\dot{\mathbf{q}}(t))\end{bmatrix}.$$

Assumption 3. The impulse force due to the impact will change the generalized velocities; however, it will not change the configuration of the system, i.e., its generalized coordinates (see page 51 [26]).

Assumption 3 indicates that the configuration of the FFSM remains the same from before (t_{i}^{-}) to right after (t_{i}^{+}) impact, that is $\mathbf{q}(t_{\mathrm{i}}^{-})=\mathbf{q}(t_{\mathrm{i}}^{+})$. Thus, to obtain a relationship between the applied impulse and the change in the generalized velocities, Eq. (10) can be integrated over the infinitesimal duration of impact $t\in[t_{\mathrm{i}}^{-},t_{\mathrm{i}}^{+}]$:

$$\int_{t_{\mathrm{i}}^{-}}^{t_{\mathrm{i}}^{+}}\mathbf{M}(\mathbf{q}(\tau))\ddot{\mathbf{q}}(\tau)\,\mathrm{d}\tau+\int_{t_{\mathrm{i}}^{-}}^{t_{\mathrm{i}}^{+}}\mathbf{c}(\mathbf{q}(\tau),\dot{\mathbf{q}}(\tau))\,\mathrm{d}\tau=-\int_{t_{\mathrm{i}}^{-}}^{t_{\mathrm{i}}^{+}}\mathbf{J}^{\top}(\mathbf{q}(\tau))\mathbf{F}_{\mathrm{e}}\delta(\tau-t_{\mathrm{i}})\,\mathrm{d}\tau,\tag{11}$$

where $\Delta t=t_{\mathrm{i}}^{+}-t_{\mathrm{i}}^{-}$ and $\Delta t\to 0$.

Lemma 1 *(Mean Value Theorem for Integrals [52]). Suppose that $u(x)$ is continuous and $v(x)$ is integrable and non-negative on interval $[a,b]$, then*

$$\int_{a}^{b}u(x)v(x)\,\mathrm{d}x=u(c)\int_{a}^{b}v(x)\,\mathrm{d}x,$$

for some c in $x \in [a, b]$.

Assuming that $\ddot{\mathbf{q}}(t)$ is non-negative and using Assumption 3, one can integrate the first term of (11) as per Lemma 1 to obtain:

$$\mathbf{M}(\mathbf{q}(t_\mathrm{i}))\int_{t_\mathrm{i}^-}^{t_\mathrm{i}^+}\ddot{\mathbf{q}}(\tau)\,\mathrm{d}\tau = \mathbf{M}(\mathbf{q}(t_\mathrm{i}))[\dot{\mathbf{q}}(t_\mathrm{i}^+) - \dot{\mathbf{q}}(t_\mathrm{i}^-)]. \tag{12}$$

To integrate the second term in (11), it is noted that the velocity dependent term in (10), $\mathbf{c}(\mathbf{q}(t), \dot{\mathbf{q}}(t))$, is discontinuous at the point of impact t_i and in order to use Lemma 1, the second term of (11) is divided into two parts as follows:

$$\begin{aligned}
&\int_{t_\mathrm{i}^-}^{t_\mathrm{i}}\mathbf{c}(\mathbf{q}(\tau),\dot{\mathbf{q}}(\tau))\,\mathrm{d}\tau + \int_{t_\mathrm{i}}^{t_\mathrm{i}^+}\mathbf{c}(\mathbf{q}(\tau),\dot{\mathbf{q}}(\tau))\,\mathrm{d}\tau = \\
&\int_{t_\mathrm{i}^-}^{t_\mathrm{i}}\mathbf{C}(\mathbf{q}(\tau),\dot{\mathbf{q}}(\tau))\dot{\mathbf{q}}(\tau)\,\mathrm{d}\tau + \int_{t_\mathrm{i}}^{t_\mathrm{i}^+}\mathbf{C}(\mathbf{q}(\tau),\dot{\mathbf{q}}(\tau))\dot{\mathbf{q}}(\tau)\,\mathrm{d}\tau = \\
&\mathbf{C}(\mathbf{q}(t_\mathrm{L}),\dot{\mathbf{q}}(t_\mathrm{L}))\int_{t_\mathrm{i}^-}^{t_\mathrm{i}}\dot{\mathbf{q}}(\tau)\,\mathrm{d}\tau + \mathbf{C}(\mathbf{q}(t_\mathrm{U}),\dot{\mathbf{q}}(t_\mathrm{U}))\int_{t_\mathrm{i}}^{t_\mathrm{i}^+}\dot{\mathbf{q}}(\tau)\,\mathrm{d}\tau = \\
&\mathbf{C}(\mathbf{q}(t_\mathrm{L}),\dot{\mathbf{q}}(t_\mathrm{L}))\underbrace{[\mathbf{q}(t_\mathrm{i}) - \mathbf{q}(t_\mathrm{i}^-)]}_{\mathbf{0}} + \mathbf{C}(\mathbf{q}(t_\mathrm{U}),\dot{\mathbf{q}}(t_\mathrm{U}))\underbrace{[\mathbf{q}(t_\mathrm{i}^+) - \mathbf{q}(t_\mathrm{i})]}_{\mathbf{0}} = \mathbf{0},
\end{aligned} \tag{13}$$

where $t_\mathrm{L} \in [t_\mathrm{i}^-, t_\mathrm{i}]$, $t_\mathrm{U} \in [t_\mathrm{i}, t_\mathrm{i}^+]$, and $\mathbf{q}(t_\mathrm{i}^+) = \mathbf{q}(t_\mathrm{i}^-) = \mathbf{q}(t_\mathrm{i})$ since there is no change in configuration at the time of impact, as per Assumption 3. Indeed, it has been stated in the literature that the Coriolis and centrifugal terms in the dynamics of multibody systems undergoing impact are non-impulsive and their integrals over the impact can be neglected [9,53,26].

Finally, the last term in (11) yields:

$$\int_{t_\mathrm{i}^-}^{t_\mathrm{i}^+}\mathbf{J}^\top(\mathbf{q}(\tau))\mathbf{F}_\mathrm{e}\delta(\tau - t_\mathrm{i})\,\mathrm{d}\tau = \mathbf{J}^\top(\mathbf{q}(t_\mathrm{i}))\int_{t_\mathrm{i}^-}^{t_\mathrm{i}^+}\mathbf{F}_\mathrm{e}\delta(\tau - t_\mathrm{i})\,\mathrm{d}\tau = \mathbf{J}^\top(\mathbf{q}(t_\mathrm{i}))\mathbf{I}_\mathrm{e}, \tag{14}$$

where $\mathbf{I}_\mathrm{e}$ is the linear impulse produced by the impact. Substituting from (12)-(14) into (11), one obtains the commonly used relationship between the change in generalized velocities and the applied impulse for the FFSM system:

$$\mathbf{M}(\mathbf{q}(t_\mathrm{i}))[\dot{\mathbf{q}}(t_\mathrm{i}^+) - \dot{\mathbf{q}}(t_\mathrm{i}^-)] = -\mathbf{J}^\top(\mathbf{q}(t_\mathrm{i}))\mathbf{I}_\mathrm{e}. \tag{15}$$

The non-negativity assumption for $\ddot{\mathbf{q}}(t)$ and $\dot{\mathbf{q}}(t)$ that was made to make use of Lemma 1 in the above derivation may not hold in all cases. It must be noted that a milder condition is keeping the same sign over the interval $[t_\mathrm{i}^-, t_\mathrm{i}^+]$ for those terms and express the same discussion for the negative part with proper changes. In the case that $\ddot{\mathbf{q}}(t)$ and $\dot{\mathbf{q}}(t)$ change sign over the impact, the conventional argument of negligible non-impulsive terms can be used instead of the Mean Value Theorem to find (15) [9,53,26].

In the context of impact resolution, we assume that the generalized velocities of the FFSM prior to impact are known. Then, Eq. (15) can be used to compute the generalized velocities right after impact with:

$$\dot{\mathbf{q}}(t_\mathrm{i}^+) = \dot{\mathbf{q}}(t_\mathrm{i}^-) - \mathbf{M}^{-1}(\mathbf{q}(t_\mathrm{i}))\mathbf{J}^\top(\mathbf{q}(t_\mathrm{i}))\mathbf{I}_\mathrm{e}, \tag{16}$$

provided that the unknown impulse $\mathbf{I}_\mathrm{e}$ can be solved for, as is described next.

Since the floating object is a rigid body, the linear and angular velocities of that will be found directly through momentum and energy conservation equations.

2.3.2. Impulse computation

To resolve the impact, that is to compute the post-impact generalized velocities of the FFSM from (16), as well as the velocity state of the floating object after impact, requires the value of the impulse $\mathbf{I}_\mathrm{e}$.

In the multibody dynamics, robotics, and graphics communities, the dynamics of multibody systems, and the modeling of contact, impact, and friction have been studied for many years [10,11,53,9]. Some mature methods have been implemented in various physics engines, such as MuJoCo, Bullet, Drake, and others. In this work, we use the discrete modeling approach to resolve the impact; therefore, conservation of linear and angular momenta of the FFSM-object system are enforced in all directions, due to the free-floating nature of the system. In addition, the assumption of frictionless elastic impact allows us to employ the conservation of energy to complete the resolution of the impact.

Conservation of linear momentum and angular momentum about the origin of the global frame for the whole FFSM-object system, from before to after impact, can be stated in the following form:

$$\begin{bmatrix}\mathcal{P}_\mathrm{FFSM}\\ \mathcal{L}_\mathrm{FFSM} + \boldsymbol{\xi}_1 \times \mathcal{P}_\mathrm{FFSM}\end{bmatrix}_{t=t_\mathrm{i}^-} = \begin{bmatrix}\mathcal{P}_\mathrm{FFSM}\\ \mathcal{L}_\mathrm{FFSM} + \boldsymbol{\xi}_1 \times \mathcal{P}_\mathrm{FFSM}\end{bmatrix}_{t=t_\mathrm{i}^+} + \begin{bmatrix}\mathcal{P}_\mathrm{o}\\ \mathcal{L}_\mathrm{o}\end{bmatrix}_{t=t_\mathrm{i}^+}, \tag{17}$$

where we made use of the fact that the floating object is stationary prior to impact and the FFSM momenta $\mathcal{P}_\mathrm{FFSM}$ and $\mathcal{L}_\mathrm{FFSM}$ are defined in (8).

Remark 3. Conservation of angular momentum for a system comprised of a space manipulator colliding with a floating object can be defined about the point of impact or about the inertial frame origin. In this work, we employ the latter for impact resolution and therefore, the angular momentum of the FFSM has been defined in (9) w.r.t. the global reference frame $\{XYZ\}$, and similarly, the angular momentum of the floating object is calculated based on the same frame as per (6).

Assumption 4. It is assumed that the impact between the FFSM and the floating object is elastic and frictionless.

The number of unknown variables of the impact problem is $12 + N$ in (17) where 6 unknowns are velocity variables of the position and orientation of the floating object, other 6 of those for the base of the FFSM, and N unknowns for the velocity of the joints of the FFSM. Equation (17) only provides 6 equations. To solve the problem, $6 + N$ unknown variables of velocities after impact are replaced with (16) which is based on unknown impact force $\mathbf{I}_\mathrm{e}$. Considering that the impact is frictionless, Assumption 4, the only component of the impact impulse force is the normal component to the surface of the floating object. Then $I_{\mathrm{e,n}}$ (with projection on fixed global frame $\mathbf{I}_\mathrm{e}$) is one unknown term that replaces $6 + N$ unknowns. Consequently, one additional equation is missing to complete the calculation, "conservation of energy."

Another equation is written using the energy of the systems before and after the impact. There might be three cases: (a) elastic impact $\Delta T(\mathbf{q}, \dot{\mathbf{q}}) = 0$ in which $T(\mathbf{q}, \dot{\mathbf{q}})$ is the kinetic energy of the whole system, the floating object, and the FFSM. In the elastic impact, the dissipation of the energy and penetration of the objects due to the impact are neglected and the conditions are assumed ideal. (b) Inelastic collision $\Delta T(\mathbf{q}, \dot{\mathbf{q}}) < 0$ in which the system loses energy through dissipation, etc. (c) Super elastic collision $\Delta T(\mathbf{q}, \dot{\mathbf{q}}) > 0$ in which the energy of the system after the impact is more than one before the collision, such as an explosion. Here in this work, a complete elastic impact has been considered which results in another equation:

$$\left[T_\mathrm{T}(\mathbf{q}, \dot{\mathbf{q}})\right]_{t=t_\mathrm{i}^-} = \left[T_\mathrm{o}(\mathbf{q}_\mathrm{o}, \dot{\mathbf{q}}_\mathrm{o}) + T_\mathrm{T}(\mathbf{q}, \dot{\mathbf{q}})\right]_{t=t_\mathrm{i}^+}. \tag{18}$$

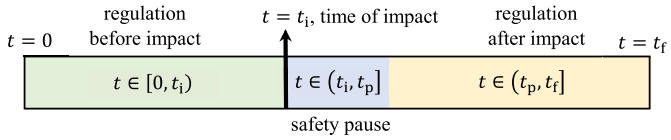

Fig. 2. Control task operation time phases: before and after impact regulation along with safety pause.

Now there are 7 equations and 7 unknowns. By solving the momentum equation (17) and the conservation of the energy (18), the linear/angular velocities of the floating object will be obtained (right after the impact), $\dot{\boldsymbol{\xi}}_{o,1}(t), \dot{\boldsymbol{\xi}}_{o,2}(t)$, along with the unknown value of the impact force. Then Eq. (16) provides all $6 + N$ unknown velocity variables of the FFSM, base and links.

2.4. Reduced-order dynamics for controller design

In this section, we formulate the reduced-order model of the FFSM system that will be required for the SDRE controller design to be presented in Section 3. This model is obtained by reducing the general equations of motion of the under-actuated FFSM system and making use of the conservation of momenta for the FFSM outside of impact. Accordingly, since the FFSM undergoes impact while performing a point-to-point maneuver, the overall control task of the FFSM will be divided into three phases as follows: (a) regulation before impact in $t \in [0, t_i)$, where recall t_i denotes the moment of impact, (b) a safety pause $t \in (t_i, t_p]$ during which actuation of FFSM is disabled, and (c) regulation to the final point of the task after impact under the post-impact conditions in $t \in (t_p, t_f]$ where t_f is the final time. The operation time phases are illustrated in Fig. 2.

To design a controller for the under-actuated FFSM, we formulate the reduced-order model in conjunction with a constraint between the base motion and the motion of the manipulator. This constraint is provided by the appropriate conservation of momenta equations for the FFSM system, formulated separately for the pre-impact and post-impact phases as detailed in the following.

2.4.1. Prior to impact $t \in [0, t_i)$

As discussed in Section 2.2, for the FFSM starting from rest conditions, the linear and angular momenta of equation (8) are conserved at zero values during this phase of the maneuver. Thus, the following kinematic relation can be obtained from (8) between the base and the arm motions of the FFSM:

$$\dot{\mathbf{q}}_b(t) = -\mathbf{M}_b^{-1}(\mathbf{q}(t))\mathbf{M}_{b,a}(\mathbf{q}(t))\dot{\mathbf{q}}_a(t). \tag{19}$$

To formulate the reduced-order equations of motion, we begin with the dynamics equations (7) simplified for the prior-to-impact conditions:

$$\mathbf{M}_b(\mathbf{q}(t))\ddot{\mathbf{q}}_b(t) + \mathbf{M}_{b,a}(\mathbf{q}(t))\ddot{\mathbf{q}}_a(t) + \mathbf{c}_b(\mathbf{q}(t), \dot{\mathbf{q}}(t)) = \mathbf{0}, \tag{20}$$

$$\mathbf{M}_{b,a}^{\top}(\mathbf{q}(t))\ddot{\mathbf{q}}_b(t) + \mathbf{M}_a(\mathbf{q}(t))\ddot{\mathbf{q}}_a(t) + \mathbf{c}_a(\mathbf{q}(t), \dot{\mathbf{q}}(t)) = \mathbf{u}(t). \tag{21}$$

Extracting $\ddot{\mathbf{q}}_b(t)$ from (20) and substituting into (21) results in:

$$\mathbf{M}_e(\mathbf{q}(t))\ddot{\mathbf{q}}_a(t) + \mathbf{c}_e(\mathbf{q}(t), \dot{\mathbf{q}}(t)) = \mathbf{u}(t), \tag{22}$$

where

$$\mathbf{M}_e(\mathbf{q}(t)) = \mathbf{M}_a(\mathbf{q}(t)) - \mathbf{M}_{b,a}^{\top}(\mathbf{q}(t))\mathbf{M}_b^{-1}(\mathbf{q}(t))\mathbf{M}_{b,a}(\mathbf{q}(t)),$$

$$\mathbf{c}_e(\mathbf{q}(t), \dot{\mathbf{q}}(t)) = \mathbf{c}_a(\mathbf{q}(t), \dot{\mathbf{q}}(t)) - \mathbf{M}_{b,a}^{\top}(\mathbf{q}(t))\mathbf{M}_b^{-1}(\mathbf{q}(t))\mathbf{c}_b(\mathbf{q}(t), \dot{\mathbf{q}}(t)).$$

For controller design, we rewrite the reduced equation of motion (22) in SS form, with the state variables of the FFSM selected as:

$$\mathbf{x}(t) = \begin{bmatrix} \mathbf{q}_a(t) \\ \dot{\mathbf{q}}_a(t) \end{bmatrix},$$

to give:

$$\dot{\mathbf{x}}(t) = \begin{bmatrix} \dot{\mathbf{q}}_a(t) \\ -\mathbf{M}_e^{-1}(\mathbf{q}(t))\mathbf{c}_e(\mathbf{q}(t), \dot{\mathbf{q}}(t)) \end{bmatrix} + \begin{bmatrix} \mathbf{0}_{N\times N} \\ \mathbf{M}_e^{-1}(\mathbf{q}(t)) \end{bmatrix} \mathbf{u}(t). \tag{23}$$

The above SS equation of the FFSM (23) depend on the base configuration and motion variables $\mathbf{q}_b(t)$ and $\dot{\mathbf{q}}_b(t)$. These are in turn computed from the kinematic constraint equation (19), which are integrated jointly with (23) to generate the information on the base motion variables.

It is emphasized that the reduced-order dynamics of this subsection, in particular, the kinematic constraint (19) applies for the pre-impact phase only. The kinematic constraint for the post-impact phase is defined next.

2.4.2. Post impact $t \in (t_p, t_f]$

As discussed in Section 2.2, the impulse generated by the collision of the FFSM with the object imparts a linear and an angular momentum to the FFSM. Equation (8) can still be employed to relate the motion of the base to the arm, with the provision that the post-impact linear momentum $\mathcal{P}_{FFSM}$ is conserved at its post-impact value; however, the angular momentum $\mathcal{L}_{FFSM}$ is not conserved and has to be updated at the sampling rate of the controller. Thus, defining the post-impact momenta of the FFSM for the third phase of the maneuver as:

$$\mathcal{M}(t) = \begin{bmatrix} \mathcal{P}_{FFSM}(t_p^+) \\ \mathcal{L}_{FFSM}(t) \end{bmatrix},$$

and solving for the base motion from (8) with the momenta $\mathcal{M}(t)$ on the left-hand side yields:

$$\dot{\mathbf{q}}_b(t) = \mathbf{M}_b^{-1}(\mathbf{q}(t))(\mathcal{M}(t) - \mathbf{M}_{b,a}(\mathbf{q}(t))\dot{\mathbf{q}}_a(t)). \tag{24}$$

Thus, in the third phase of the maneuver, equation (24) is used to compute the motion of the base in conjunction with the reduced-order dynamics equations (23) for the SDRE regulation controller.

Although the reduced-order dynamics can be employed for the controller design for the post-impact phase of the regulation maneuver, the following comments are in order. In the absence of an impact phase and assuming the FFSM begins its motion from rest, the SDRE controller can regulate the end-effector motion to a final stationary pose. However, following impact which imparts a non-zero momentum to the FFSM, the actuation of the manipulator alone is not sufficient to complete the point-to-point maneuver: without external input to the base by using thrusters, it is not possible to compensate for the conserved non-zero momentum of the system with actuation of the manipulator alone.

To summarize, the OSDRE controller for the manipulator formulated in the next section, or any other controller of the arm, cannot complete the point-to-point regulation with the FFSM experiencing a collision part way. The FFSM will invariably drift away, with the drift rate depending on its inertial properties and the magnitude of the impulse. This implies that the existence of thrusters on the base of the FFSM is essential. In Section 4.4, we will demonstrate the use of base thrusters during the safety pause, to reduce the linear momentum of the base to zero, before engaging the OSDRE controller for the arm in the third phase of the maneuver.

***Main result**: An initially static FFSM without thrusters on the base cannot finish the regulation control task no matter what controller it has if the slightest impact in regulation happens.*

Clearly, this subject could be expanded for capturing objects in space, and contact cases for the manipulators and indicates the necessity of thrusters to keep the FFSM in the same local location (orbit).

3. Output feedback SDRE control

Consider a k-th-order system of differential equations for a dynamical system

$$\mathbf{r}^{(k)}(t) = \boldsymbol{\eta}\left(\mathbf{r}(t), \dot{\mathbf{r}}(t), \cdots, \mathbf{r}^{(k-1)}(t), \mathbf{u}(t)\right), \tag{25}$$

where $\mathbf{u}(t) \in \mathbb{R}^m$ is the input vector, m is the number of actuators, $\mathbf{r}(t) \in \mathbb{R}^n$ is the generalized coordinate, and n is the DoF of the system. The state-vector of the system is chosen as $\mathbf{x}(t) = [\mathbf{r}^\top(t), \dot{\mathbf{r}}^\top(t), \cdots, (\mathbf{r}^{(k-1)}(t))^\top]^\top$ and it leads to the SS representation of the system (25), states and outputs [42]:

$$\begin{aligned}\dot{\mathbf{x}}(t) =& \mathbf{f}(\mathbf{x}(t)) + \mathbf{g}(\mathbf{x}(t), \mathbf{u}(t)),\\ \mathbf{y}(t) =& \mathbf{h}(\mathbf{x}(t)),\end{aligned} \tag{26}$$

in which

$$\mathbf{f}(\mathbf{x}(t)) = \begin{bmatrix} \dot{\mathbf{r}}(t) \\ \ddot{\mathbf{r}}(t) \\ \vdots \\ \boldsymbol{\eta}_{\mathrm{x}}\left(\mathbf{r}(t), \dot{\mathbf{r}}(t), \cdots, \mathbf{r}^{(k-1)}(t)\right) \end{bmatrix},$$

$$\mathbf{g}(\mathbf{x}(t), \mathbf{u}(t)) = \begin{bmatrix} \mathbf{0} \\ \mathbf{0} \\ \vdots \\ \boldsymbol{\eta}_{\mathrm{u}}\left(\mathbf{r}(t), \dot{\mathbf{r}}(t), \cdots, \mathbf{r}^{(k-1)}(t), \mathbf{u}(t)\right) \end{bmatrix},$$

are vector-valued functions that satisfy the local Lipschitz condition (continuous and smooth), $\mathbf{y}(t) \in \mathbb{R}^p$ is the output vector, moreover, $\mathbf{f}(\mathbf{x}(t)) : \mathbb{R}^{kn} \to \mathbb{R}^{kn}$, $\mathbf{g}(\mathbf{x}(t), \mathbf{u}(t)) : \mathbb{R}^{kn} \times \mathbb{R}^m \to \mathbb{R}^{kn}$, and $\mathbf{h}(\mathbf{x}(t)) : \mathbb{R}^{kn} \to \mathbb{R}^p$ are held.

The following assumptions are made to transform state feedback dynamics (26) into output feedback form:

A1. The output vector's components $\mathbf{y}(t)$ in (26) are non-singular in $t \in [0, t_{\mathrm{f}}]$.
A2. rank $\left[\frac{\partial \mathbf{g}(\mathbf{x}(t), \mathbf{u}(t))}{\partial \mathbf{u}(t))}\right] = m$ which shows that the inputs are independent [54].
A3. The output terms are differentially independent.
A4. $m \geq p$.
A5. The output component $y_i(t)$ shows a combination of generalized coordinates in i-th row of $\mathbf{h}(\mathbf{x}(t))$, specifically, $y_i(t)$ has at least one term of $q_i(t)$.

Lemma 2. *Derivation of the output dynamics, k-times, reveals the independent control terms in the output dynamics [42].*

A1-A5 and Lemma 2 transform the dynamics (26) into output feedback design. The state variables of the output feedback dynamics are:

$$\mathbf{z}(t) = \begin{bmatrix} \mathbf{y}(t) \\ \dot{\mathbf{y}}(t) \\ \vdots \\ \mathbf{y}^{(k-1)}(t) \end{bmatrix}. \tag{27}$$

The SS representation of the output dynamics is found by computing the time-derivative of (27):

$$\dot{\mathbf{z}}(t) = \mathbf{A}(\mathbf{x}(t), \mathbf{z}(t))\mathbf{z}(t) + \mathbf{B}(\mathbf{x}(t))\mathbf{u}(t), \tag{28}$$

where $\mathbf{B}(\mathbf{x}(t)) : \mathbb{R}^{kn} \to \mathbb{R}^{kp \times m}$ and $\mathbf{A}(\mathbf{x}(t), \mathbf{z}(t)) : \mathbb{R}^{kn} \times \mathbb{R}^{kp} \to \mathbb{R}^{kp \times kp}$ are output and state-dependent coefficient (OSDC) parameterization of the output dynamics.

Based on Lemma 2, the derivation of $\mathbf{y}^{(k)}(t)$ in (28) generates an affine control input vector

$$\begin{aligned}\mathbf{y}^{(k)}(t) =& \boldsymbol{\alpha}(\mathbf{x}(t))\mathbf{r}^{(k)}(t) + \boldsymbol{\beta}(\mathbf{x}(t)) =\\ & \boldsymbol{\alpha}(\mathbf{x}(t))\boldsymbol{\eta}_{\mathrm{x}}(\mathbf{x}(t)) + \boldsymbol{\beta}(\mathbf{x}(t)) + \boldsymbol{\alpha}(\mathbf{x}(t))\boldsymbol{\eta}_{\mathrm{u}}(\mathbf{x}(t), \mathbf{u}(t)) =\\ & \boldsymbol{\alpha}(\mathbf{x}(t))\boldsymbol{\eta}_{\mathrm{x}}(\mathbf{x}(t)) + \boldsymbol{\beta}(\mathbf{x}(t)) + \boldsymbol{\alpha}(\mathbf{x}(t))\mathbf{E}_{\mathrm{u}}(\mathbf{x}(t))\mathbf{u}(t),\end{aligned} \tag{29}$$

where $\boldsymbol{\alpha}(\mathbf{x}(t)) : \mathbb{R}^{kn} \to \mathbb{R}^{p \times n}$, $\boldsymbol{\beta}(\mathbf{x}(t)) : \mathbb{R}^{kn} \to \mathbb{R}^p$, and $\mathbf{E}_{\mathrm{u}}(\mathbf{x}(t)) : \mathbb{R}^{kn} \to \mathbb{R}^{n \times m}$. Equation (29) provides the OSDC parameterization:

$$\begin{aligned}\mathbf{A}(\mathbf{x}(t), \mathbf{z}(t)) =& \begin{bmatrix} \mathbf{0}_{p(k-1) \times p} & \mathbf{I}_{p(k-1) \times p(k-1)} \\ \mathbf{0}_{p \times p(k-1)} & \left[\{\boldsymbol{\alpha}(\mathbf{x}(t))\boldsymbol{\eta}_{\mathrm{x}}(\mathbf{x}(t)) + \boldsymbol{\beta}(\mathbf{x}(t))\}[\mathbf{y}^{(k-1)}(t)]^\dagger\right]_{p \times p} \end{bmatrix},\\ \mathbf{B}(\mathbf{x}(t)) =& \begin{bmatrix} \mathbf{0}_{p(k-1) \times m} \\ \left[\boldsymbol{\alpha}(\mathbf{x}(t))\mathbf{E}_{\mathrm{u}}(\mathbf{x}(t))\right]_{p \times m} \end{bmatrix},\end{aligned} \tag{30}$$

where $[\mathbf{y}^{(k-1)}(t)]^\dagger$ is the generalized inverse of $\mathbf{y}^{(k-1)}(t)$.

Condition 1. $\{\mathbf{A}(\mathbf{x}(t), \mathbf{z}(t)), \mathbf{B}(\mathbf{x}(t))\}$ is a completely controllable OSDC pair [42].

The cost function of the OSDRE is defined as:

$$J = \frac{1}{2}\int_0^\infty \{\mathbf{u}^\top(t)\mathbf{R}(\mathbf{x}(t))\mathbf{u}(t) + \mathbf{z}^\top(t)\mathbf{Q}(\mathbf{x}(t))\mathbf{z}(t)\}\,\mathrm{d}t, \tag{31}$$

in which the states are penalized by the symmetric positive-semi-definite weighting matrix $\mathbf{Q}(\mathbf{x}(t)) : \mathbb{R}^{kn} \to \mathbb{R}^{kp \times kp}$, and the inputs are penalized by symmetric positive definite weighting matrix $\mathbf{R}(\mathbf{x}(t)) : \mathbb{R}^{kn} \to \mathbb{R}^{m \times m}$.

Condition 2. $\{\mathbf{A}(\mathbf{x}(t), \mathbf{z}(t)), \mathbf{Q}^{1/2}(\mathbf{x}(t))\}$ is a completely observable OSDC pair, where $\mathbf{Q}^{1/2}(\mathbf{x}(t))$ is the Cholesky decomposition of $\mathbf{Q}(\mathbf{x}(t))$ in (31) [42].

The input law of the OSDRE is

$$\mathbf{u}(t) = -\mathbf{R}^{-1}(\mathbf{x}(t))\mathbf{B}^\top(\mathbf{x}(t))\mathbf{K}(\mathbf{x}(t), \mathbf{z}(t))\mathbf{z}(t), \tag{32}$$

in which $\mathbf{K}(\mathbf{x}(t), \mathbf{z}(t)) : \mathbb{R}^{kn} \times \mathbb{R}^{kp} \to \mathbb{R}^{kp \times kp}$ is the positive-definite solution to the OSDRE (a symmetric gain):

$$\begin{aligned}&\mathbf{A}^\top(\mathbf{x}(t), \mathbf{z}(t))\mathbf{K}(\mathbf{x}(t), \mathbf{z}(t)) + \mathbf{K}(\mathbf{x}(t), \mathbf{z}(t))\mathbf{A}(\mathbf{x}(t), \mathbf{z}(t)) + \mathbf{Q}(\mathbf{x}(t)) -\\ &\mathbf{K}(\mathbf{x}(t), \mathbf{z}(t))\mathbf{B}(\mathbf{x}(t))\mathbf{R}^{-1}(\mathbf{x}(t))\mathbf{B}^\top(\mathbf{x}(t))\mathbf{K}(\mathbf{x}(t), \mathbf{z}(t)) = \mathbf{0}.\end{aligned} \tag{33}$$

4. Case study: FFSM with a three-DoF manipulator

4.1. System definition

The implementation of the OSDRE controller, the computations of impact impulse and the velocity of the states after impact, and the simulation of the complete system dynamics are carried out for an FFSM with a three-DoF arm, moving from the initial to the final configurations, as illustrated in Fig. 3. The state-space dynamics of the floating object experiencing impact at t_{i} is simplified to the following equations for planar motion:

$$\dot{\mathbf{x}}_{\mathrm{o}}(t) = \begin{bmatrix} \dot{x}_{\mathrm{o}}(t) \\ \dot{y}_{\mathrm{o}}(t) \\ \dot{\psi}_{\mathrm{o}}(t) \\ \ddot{x}_{\mathrm{o}}(t) \\ \ddot{y}_{\mathrm{o}}(t) \\ \ddot{\psi}_{\mathrm{o}}(t) \end{bmatrix} = \begin{bmatrix} 0 & 0 & 0 & 1 & 0 & 0 \\ 0 & 0 & 0 & 0 & 1 & 0 \\ 0 & 0 & 0 & 0 & 0 & 1 \\ 0 & 0 & 0 & 0 & 0 & 0 \\ 0 & 0 & 0 & 0 & 0 & 0 \\ 0 & 0 & 0 & 0 & 0 & 0 \end{bmatrix} \begin{bmatrix} x_{\mathrm{o}}(t) \\ y_{\mathrm{o}}(t) \\ \psi_{\mathrm{o}}(t) \\ \dot{x}_{\mathrm{o}}(t) \\ \dot{y}_{\mathrm{o}}(t) \\ \dot{\psi}_{\mathrm{o}}(t) \end{bmatrix} + \begin{bmatrix} 0 & 0 & 0 \\ 0 & 0 & 0 \\ 0 & 0 & 0 \\ 1/m_{\mathrm{o}} & 0 & 0 \\ 0 & 1/m_{\mathrm{o}} & 0 \\ 0 & 0 & 1/I_{zz,\mathrm{o}} \end{bmatrix} \begin{bmatrix} F_{\mathrm{e},x}\delta(t - t_{\mathrm{i}}) \\ F_{\mathrm{e},y}\delta(t - t_{\mathrm{i}}) \\ \tau_{\mathrm{e},\psi}\delta(t - t_{\mathrm{i}}) \end{bmatrix}.$$

The mass of the object is $m_{\mathrm{o}} = 5$ kg and it is modeled as a box with 1 m side length and centroidal moment of inertia of $I_{zz,\mathrm{o}} = 0.8333$ kg-m^2. Prior to impact, the object is stationary and is located on the way of the path of the gripper of the FFSM, at the initial position and orientation defined as (CoM of the object):

$$[x_{\mathrm{o}}(0), y_{\mathrm{o}}(0), \psi_{\mathrm{o}}(0)]^\top = [3.5, -0.5, 0]^\top (\mathrm{m}, \mathrm{rad}).$$

The impact will happen on the right side of the object, $x_{\mathrm{i}} = 4$ m; however, y_{i} depends on the position of the end-effector when it hits the object. If it hits the object below the CoM, the object will rotate clockwise, and if above the CoM, counter-clockwise. Following impact, the object responds to the impulsive force and moment about its CoM, which impart a translational and rotational motion to the object.

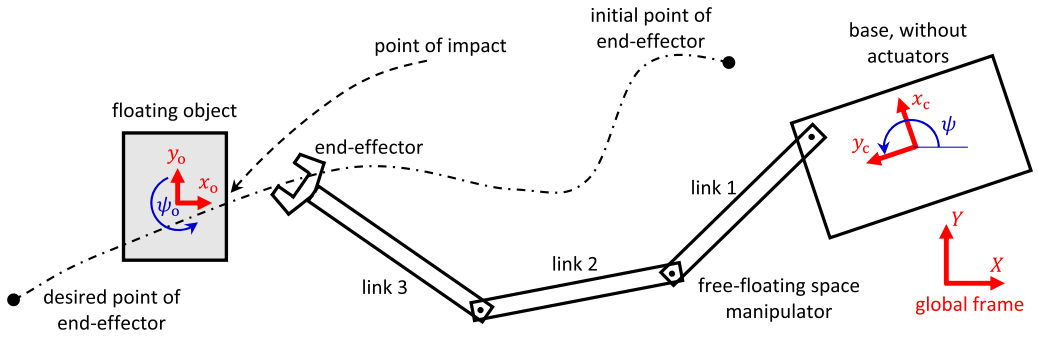

Fig. 3. The schematic view of the case study of the simulation, an FFSM with a three-DoF manipulator on the way of a collision.

Table 1
The parameters of the FFSM [42].

description	parameter	unit	value
mass of links	m_1, m_2, m_3	kg	2
mass of load	m_p	kg	1
mass of base	m_b	kg	5
length of links	a_1, a_2, a_3	m	2
center-of-mass of links	$a_{c,1}, a_{c,2}, a_{c,3}$	m	1
moment of inertia of links	$I_{zz,1}, I_{zz,2}, I_{zz,3}$	kg – m^2	0.6667
moment of inertia of base	$I_{zz,b}$	kg – m^2	2.0833
stall torque of motors	$u_{1,\text{stall}}, u_{2,\text{stall}}, u_{3,\text{stall}}$	N – m	14
no-load speed of motors	$\omega_{1,\text{nl}}, \omega_{2,\text{nl}}, \omega_{3,\text{nl}}$	rad/s	0.54

The generalized coordinates of the FFSM considering the planar geometry and the DoF of the manipulator in Fig. 3 are:

$$\mathbf{q}_b(t) = [x_c(t), y_c(t), \psi(t)]^\top,$$

$$\mathbf{q}_a(t) = [q_1(t), q_2(t), q_3(t)]^\top,$$

which define the generalized coordinates of FFSM as

$$\mathbf{q}(t) = \begin{bmatrix} \mathbf{q}_b(t) \\ \mathbf{q}_a(t) \end{bmatrix},$$

and $N = 3$. The physical parameters of the FFSM are presented in Table 1.

The output of the FFSM system is $\mathbf{y}(t) = \mathbf{h}(\mathbf{x}(t)) = [x_e(\mathbf{q}(t)), y_e(\mathbf{q}(t))]^\top$ with $p = 2$ where $(x_e(\mathbf{q}(t)), y_e(\mathbf{q}(t)))$ are the 2D Cartesian coordinates of the end-effector of the FFSM [42]. For the second-order dynamics of FFSM, $k = 2$, and applying the dynamics equation (23) results in the following OSDC parameterization (30):

$$\mathbf{A}(\mathbf{x}, \mathbf{z}) = \begin{bmatrix} \mathbf{0}_{2\times2} & \mathbf{I}_{2\times2} \\ \mathbf{0}_{2\times2} & \left[\{\boldsymbol{\beta}(\mathbf{x}) - \boldsymbol{\alpha}(\mathbf{x})\mathbf{M}_e^{-1}(\mathbf{x})\mathbf{c}_e(\mathbf{x})\}[\dot{\mathbf{y}}]^+\right]_{2\times2} \end{bmatrix},$$

$$\mathbf{B}(\mathbf{x}) = \begin{bmatrix} \mathbf{0}_{2\times3} \\ \left[\boldsymbol{\alpha}(\mathbf{x})\mathbf{M}_e^{-1}(\mathbf{x})\right]_{2\times3} \end{bmatrix}.$$

The tuning weighting matrices of states and inputs (for before impact $t \in [0, t_i)$) are selected as

$$\mathbf{R} = \mathbf{I}_{3\times3},$$

$$\mathbf{Q} = \text{diag}(1, 1, 0.5, 0.5),$$

and for the after-impact $t \in (t_p, t_f]$, the weighting matrix of inputs is reduced to enhance the controller in regulation to recover from the deviation due to the impact:

$$\mathbf{R} = 0.1\ \mathbf{I}_{3\times3}.$$

The initial position of the gripper is set to $\mathbf{y}(0) = [7.5, 1.5]^\top$(m) and the initial angle for the third link is 0.1 rad while the initial position and orientation of the base are set to:

$$[x_c(0), y_c(0), \psi(0)]^\top = [5, -1.75, 0.1]^\top(\text{m}, \text{rad}).$$

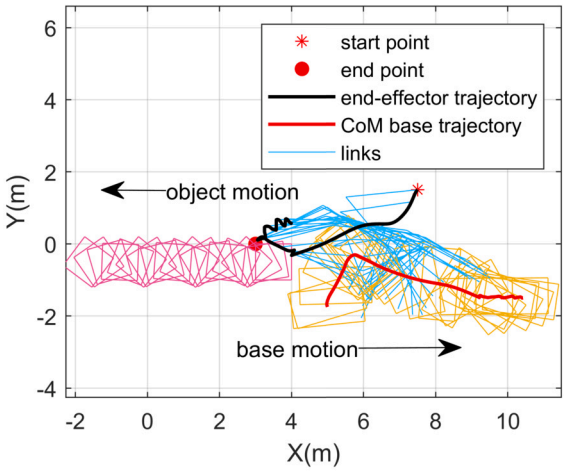

Fig. 4. Simulated configurations and trajectory of FFSM and object: the object moves away due to the impact impulse and lack of actuator for compensation of the deviation. The ***video presentation*** of the reaction and the impact are illustrated as the supplementary material of the paper.

The final desired location of the end-effector is $\mathbf{y}(t_f) = [3, 0]^\top$ m and the total time for the control task is set to $t_f = 30$ s.

As described earlier, the control task is set up in three phases, as illustrated in Fig. 2. The first pre-impact phase ends upon impact detection. In our simulation, the impact detection is carried out by checking the distance between the gripper and the right side of the floating object: if the distance is < 1 mm, the impact is declared, the simulation switches to the impact resolution and the manipulator controller is turned off. The impact solution gives the initial conditions for the post-impact phase, with the FFSM and the floating object reacting to the collision for 2.3 s as a safety pause. This concludes the second phase of the simulation. At the beginning of the third phase, the OSDRE controller re-starts its regulation of the FFSM and is constrained based on (24).

The motors of the manipulator are bounded by [55]:

$$\begin{aligned} u_{i,\max}(t) &= u_{i,\text{stall}} - \frac{u_{i,\text{stall}}}{\omega_{i,\text{nl}}}\dot{q}_i(t), \\ u_{i,\min}(t) &= -u_{i,\text{stall}} - \frac{u_{i,\text{stall}}}{\omega_{i,\text{nl}}}\dot{q}_i(t), \end{aligned} \tag{34}$$

where $u_{i,\text{stall}}$ is the stall torque of the motor of link i, and $\omega_{i,\text{nl}}$ is the corresponding no-load speed. Equations (34) define the upper and lower bounds for joint torque plots, such as Figs. 7a, 7b and 8.

4.2. Simulation: baseline scenario

The results are presented for the baseline scenario as per system definition and control phases described in Section 4.1. Since the contact surface of the floating object is perpendicular to the X-axis, the only com-

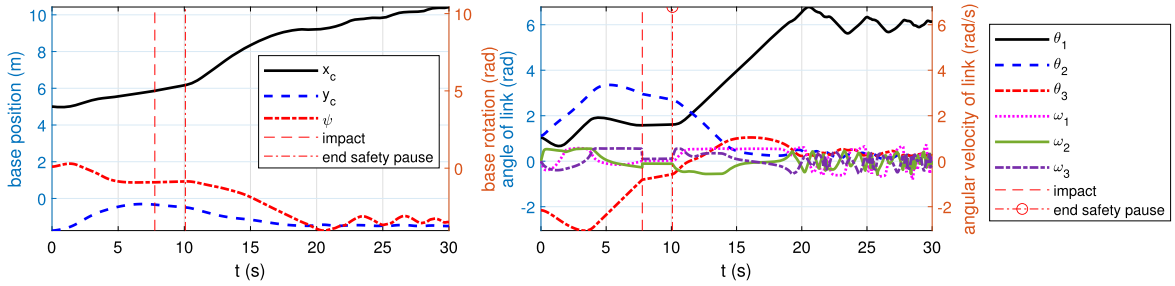

(a) The base. (b) The manipulator.

Fig. 5. (a) The orientation and position of the base of the FFSM. (b) The angles and velocities of the arm on the FFSM.

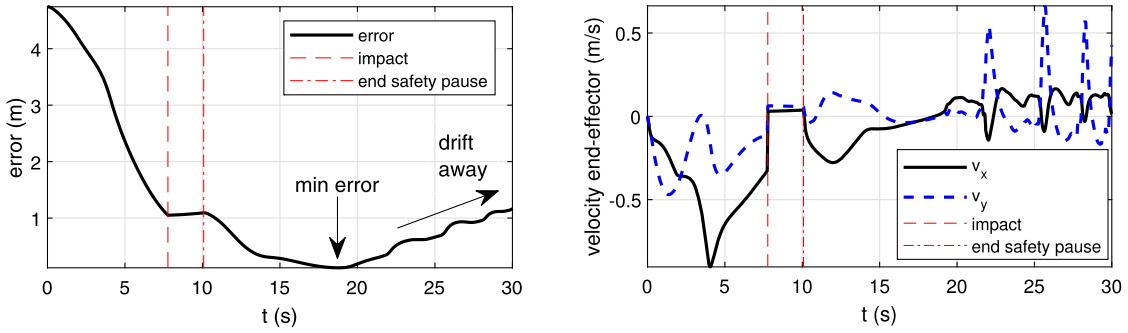

(a) End-effector error. (b) End-effector velocity.

Fig. 6. (a) End-effector error of the FFSM in the impact simulation. (b) End-effector velocity of the FFSM in the impact simulation.

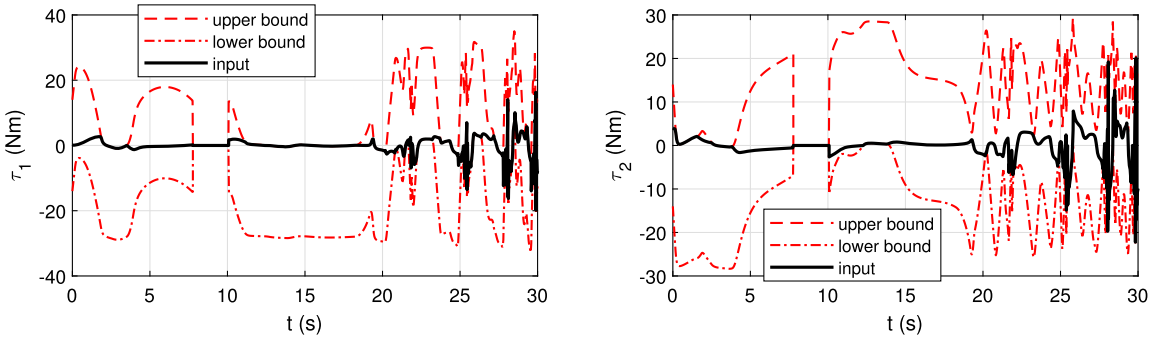

(a) The first joint. (b) The second joint.

Fig. 7. (a) The torque of the first link. (b) The torque of the second link.

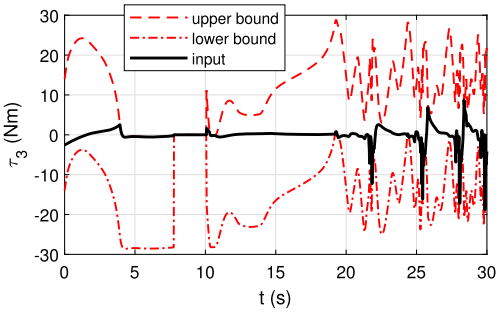

Fig. 8. The input torque of the third joint.

ponent of the impact impulse is in the X direction $\mathbf{I}_e = [I_{e,n}, 0]^\top$(Ns). Impact happens at 7.77 s of the simulation and considering the velocities and positions of the system before the impact, Eq. (16) provides the corresponding values after the impact as a function of the normal component of impulse. The detailed expressions related to the impact resolution are included in the Appendix for future validations.

The trajectories of the FFSM's gripper and the base, as well as the evolution of the system configuration for the whole motion, are illustrated in Fig. 4. The position variables of the base CoM and the rotation of the base are plotted in Fig. 5a. The arm's angles and joint rates are presented in Fig. 5b. The position error of the gripper along with the velocity of the gripper are illustrated in Figs. 6a and 6b, respectively. The input torque signals are also presented in Figs. 7a, 7b, and 8.

The end-effector starts from the initial position and collides with the static floating object at 7.77 s. It bounces back during the 2.3 s safety pause and, subsequently is regulated towards the final point, as can be seen in Fig. 4. The impact point is $[x_e(\mathbf{q}(t_i)), y_e(\mathbf{q}(t_i))]^\top = [4.009, -0.3172]^\top$ m. Considering that the CoM of the object in y_o-axis is -0.5, the end-effector hits the object above the CoM and results in counter-clockwise rotation. As expected, the joint rates of the manipulator and the end-effector velocities change discontinuously as per discrete modeling of impact, while the corresponding position variables (joint angles and end-effector positions) remain continuous, Fig. 5b. The

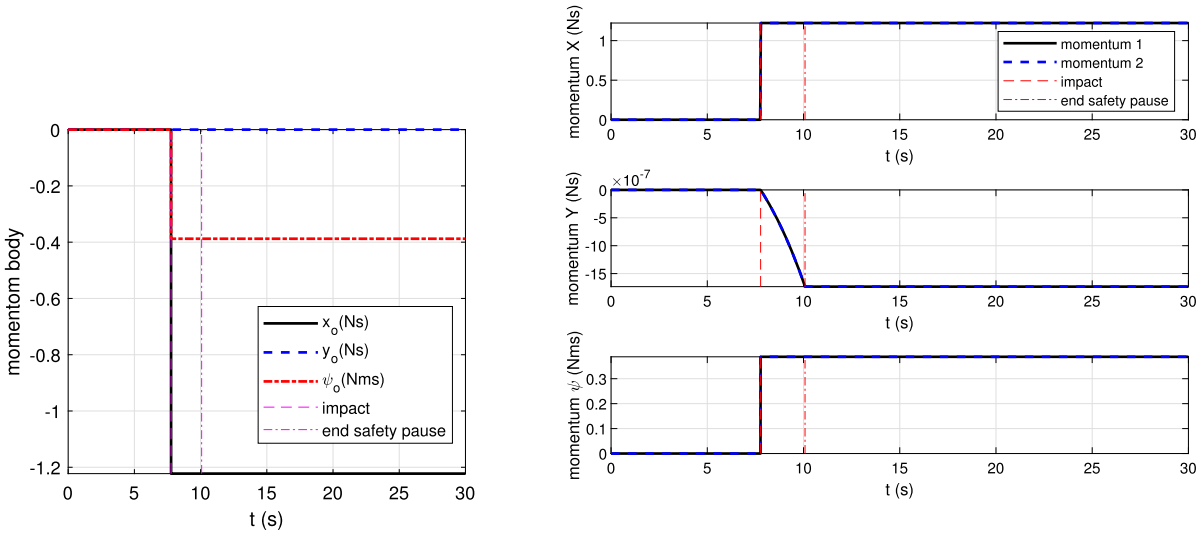

(a) The floating object. (b) The FFSM.

Fig. 9. (a) The linear momentum components and angular momentum of the object, the latter about the origin of the inertial frame. Note that the angular momentum of the object is negative even though it rotates counter-clockwise, i.e., in the positive direction. (b) The linear momentum components and angular momentum of the FFSM, the latter about the origin of the inertial frame.

end-effector error is reduced progressively from the large initial error of 5 m to 0.118 m which is less than 2.3% of the travel distance, indicating that the FFSM regulated the gripper towards the endpoint after the impact. After the impact during the safety pause of 2.3 s, the actuators are turned off, with zero signals showing during this safety zone, Figs. 7a, 7b, and 8. The linear impulse imparted to the object ($I_{e,n} = -1.2226$ Ns) produces the expected object motion immediately after impact. In particular, the object moves to the left while rotating counter-clockwise, the latter in accord with the angular impulse of 0.2235 Nms (counter-clockwise) since the impact occurs above the CoM of the object along the y_o-axis.

The responses of the momenta and energy for the FFSM and the object provide the necessary validation of the correctness of the computations. Outside of impact, the momenta (linear and angular about the origin of the inertial frame) of the object and those of the FFSM must be conserved. Since the object and FFSM are initially at rest, the conserved values are at zero until a collision occurs between them. Following the collision, momenta are imparted to both FFSM and the object and are again conserved at their post-impact values for both systems. The momenta of the object and the FFSM are plotted in Figs. 9a and 9b, respectively. The momentum generated by the impact on FFSM is added to the FFSM system and remains constant throughout the second and third control phases, Fig. 9b. This generated momentum manifests itself in the drifting motion of the FFSM, in this particular scenario to the right, and this motion will continue indefinitely, unless countered with external actuation on the base (e.g., with thrusters). This drift in the motion of the FFSM is observable in the end-effector position error plot, Fig. 6a. The minimum error reached is 0.118 m, but it increases resulting in a final error of 1.169 m at the end of the simulation in 30 s. If the simulation is continued, this error will increase as well and, the FFSM will be lost in space, similarly to the floating object. As alluded to earlier, this confirms the necessity of thrusters on the base of FFSM and the required switching to a free-flying control mode after the FFSM experiences a collision.

We also note that two responses representing the linear and angular momenta of the FFSM are included in Fig. 9b. This is done to provide additional validation of the momentum equation (17) (momentum 1 in Fig. 9b.) The comparison is done w.r.t. computing the linear and angular momenta of FFSM by summing individual momenta of each body/link about the origin of the global reference frame (momentum 2).

Fig. 10a plots the kinetic (total) energy of the FFSM and Fig. 10b shows the kinetic (total) energy of the object. The energy response of the FFSM indicates a higher power consumption by the motors in the first phase of the controller, when the initial errors are higher, while in the third phase of the regulation control, closer to the endpoint, we expect a lower power consumption by the motors. As expected, the energy remained constant during the safety pause when the actuators were turned off.

4.3. Simulation: FFSM response to impact without post-impact actuation

In this section, we are interested in exploring the response of the FFSM in a scenario where the controller is not reactivated after the safety pause so that we can observe the unactuated post-impact response of the FFSM. Does it move to the right steadily after the impact? Simulation results are presented for the system with the same parameters and conditions as in Section 4.2 with the only change of keeping the actuators turned off after the impact, until the end of the simulation. The motion of the robot and the floating object are shown in Fig. 11 and the error of the end-effector is plotted in Fig. 12a.

The approximately 6 m motion of the floating object to the left and a similar overall translation of the FFSM base to the right are visible in Fig. 11. This simulation shows that the impact that occurred with the last link of the FFSM is distributed to the previous links and the carrier of the arm. The actuator input at the third joint of the FFSM is plotted in Fig. 12b, to confirm that the manipulator is unactuated after the impact with the object.

4.4. Free-flying in safety pause: compensating for impact momentum

We had stated in Section 2.4.2 that the momentum generated by the impact will not allow the FFSM to complete its regulation task because of the drift it will experience following the impact. In this subsection, we briefly describe how to incorporate the free-flying phase in the space manipulator control in order to compensate for the generated momentum and to address this issue. Thus, by activating thrusters and reaction wheels of the FFSM, the robot switches to a free-flying mode. We consider the presented simulation scenario as in the previous sections, except that now, we turn on the base actuators during the safety pause $t \in (t_i, t_p]$ and actuate the manipulator as well. For the before-impact, and after-safety-pause control loops, the OSDRE controller as

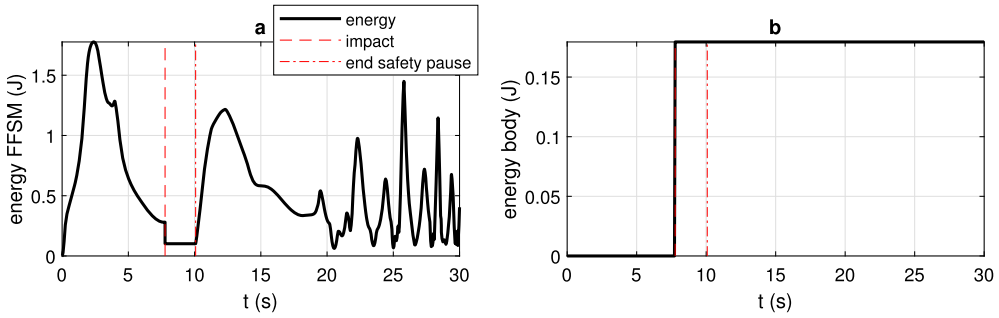

Fig. 10. The energy of the FFSM and the floating object in simulation.

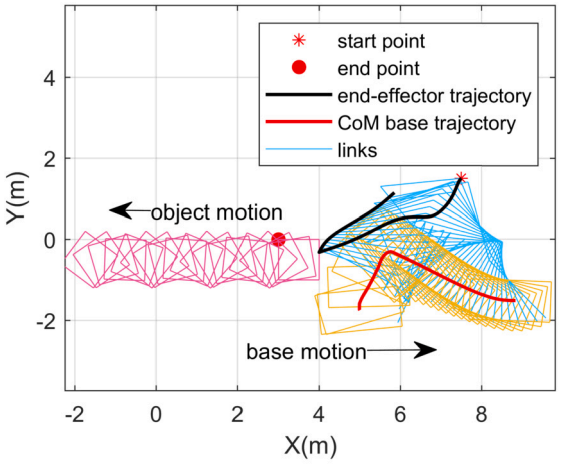

Fig. 11. The comparison between the floating object and the FFSM, in reaction to impact, showing the whole range of motion, without actuation after impact. The ***video presentation*** of the reaction and the impact is illustrated as the supplementary material of the paper.

presented before will be used, while the base thrusters are off. The objective for the free-flying mode is to regulate the system immediately after impact, by using both the base and the arm actuators, to the system configuration right before impact, ideally with zero momentum (static state). Therefore, the thrusters and the reaction wheel are controlled with proportional-derivative (PD) controllers as follows:

$$\mathbf{u}_{\mathrm{t}}(t) = -\mathbf{K}_{\mathrm{p,t}} \begin{bmatrix} x_{\mathrm{c}}(t) - x_{\mathrm{c}}(t_{\mathrm{i}}) \\ y_{\mathrm{c}}(t) - y_{\mathrm{c}}(t_{\mathrm{i}}) \end{bmatrix} - \mathbf{K}_{\mathrm{d,t}} \begin{bmatrix} \dot{x}_{\mathrm{c}}(t) \\ \dot{y}_{\mathrm{c}}(t) \end{bmatrix},$$

$$u_{\mathrm{r}}(t) = -K_{\mathrm{p,r}}(\psi(t) - \psi(t_{\mathrm{i}})) - K_{\mathrm{d,r}}\dot{\psi}(t),$$

where $\mathbf{u}_{\mathrm{t}}(t)$ and $u_{\mathrm{r}}(t)$ are the control inputs of thrusters and reaction wheel of the base, respectively, $\mathbf{K}_{\mathrm{p,t}} = 50\ \mathbf{I}_{2\times 2}$ is the proportional gain matrix of the thrusters, $\mathbf{K}_{\mathrm{d,t}} = 0.75\ \mathbf{K}_{\mathrm{p,t}}$ is the derivative gain, $K_{\mathrm{p,r}} = 200$ and $K_{\mathrm{d,r}} = 0.75\ K_{\mathrm{p,r}}$ are the proportional and derivative gains of the reaction wheel, respectively. Another set of PD controllers is designed for the arm to counteract the generated momentum of the arm:

$$\mathbf{u}_{\mathrm{a}}(t) = -\mathbf{K}_{\mathrm{p,a}}(\mathbf{q}_{\mathrm{a}}(t) - \mathbf{q}_{\mathrm{a}}(t_{\mathrm{i}})) - \mathbf{K}_{\mathrm{d,a}}\dot{\mathbf{q}}_{\mathrm{a}}(t),$$

where $\mathbf{K}_{\mathrm{p,a}} = 150\ \mathbf{I}_{3\times 3}$ is the proportional gain matrix of the arm controller and $\mathbf{K}_{\mathrm{d,a}} = 0.75\ \mathbf{K}_{\mathrm{p,a}}$ is the derivative gain. The desired base and joint velocities in the PD controllers are set to zero to bring the system to a static state after the impact.

The base thrusters' inputs are limited according to:

$$\mathbf{u}_{\mathrm{t}}(t) = \begin{cases} u_{\mathrm{t,max}}\mathrm{sign}(\mathbf{u}_{\mathrm{t}}(t)) & |\mathbf{u}_{\mathrm{t}}(t)| > \mathbf{u}_{\mathrm{t,threshold}}, \\ \mathbf{0} & |\mathbf{u}_{\mathrm{t}}(t)| \le \mathbf{u}_{\mathrm{t,threshold}}, \end{cases}$$

to emulate on-off actuation, with $u_{\mathrm{t,max}} = 50$ N and $\mathbf{u}_{\mathrm{t,threshold}} = [1, 1]^{\mathrm{T}}$ N. The reaction wheel is bounded similarly to the motors of the arm in (34) where the stall torque of the reaction wheel is set as 20 N-m and the no-load speed as 2 rad/s. To allow sufficient time for momentum compensation, the duration of the safety pause is increased to 4.6 s.

The resulting system evolution and the end-effector path are illustrated in Fig. 13, demonstrating the motion of the robot without a final drift. The end-effector error is plotted in Fig. 14a and the velocity of the end-effector is plotted in Fig. 14b. The final regulation error of the end-effector is 0.3 mm, significantly lower than in the free-floating condition. In addition, and more importantly than the reduction in the regulation error is the nearly static position of the robot after the regulation task. Therefore, the robot will not drift and will remain in the same operational zone after completing the point-to-point task. The momenta of the FFSM system are shown in Fig. 15 which demonstrate the reduction of the impact momenta to approximately zero values during the free-flying mode. The thruster signals and the reaction wheel torque are plotted in Fig. 16.

4.5. Asymptotic convergence, velocity of the end-effector

The OSDRE controller ensures local asymptotic convergence of the system states towards the endpoint [56]. This allows us to highlight another aspect of the regulation of FFSM undergoing a collision during the point-to-point maneuver. The location of the object along the nominal end-effector path from its initial to the final position has a direct effect on the impact velocity of the collision. The control law of the OSDRE (32) indicates that the error vector is multiplied by the control gain, and since at the beginning of the regulation, the error is at its maximum value, the largest inputs will be applied to the system dynamics in the beginning of the maneuver. Hence, the rate of convergence is close to the maximum possible bound. As the end-effector approaches its final goal, the regulation error becomes smaller and the speed of convergence is reduced. These considerations imply that if the gripper collides with the object at the beginning of the point-to-point motion, the speed of the gripper is high which results in a larger impact force. On the contrary, if the gripper collides with the object close to the final goal, it moves slower and the impact between the FFSM and the object is weaker, resulting in only a small bounce.

The above aspects are demonstrated here by simulating a scenario similar to that considered in Section 4.4, but with a change in the position of the object: here, the object is placed at

$$[x_{\mathrm{o}}(0), y_{\mathrm{o}}(0), \psi_{\mathrm{o}}(0)]^{\mathrm{T}} = [2.6, 0, 0]^{\mathrm{T}}(\mathrm{m, rad}).$$

Simulating the system response, the end-effector error and velocity are presented in Figs. 17a and 17b, respectively. It is noted that the end-effector error is nearly null when it impacts the floating object; then, in response to the impact, the error increases and is regulated back toward the final goal point. The velocity of the gripper also shows very small values for x, y directions, $\dot{x}_{\mathrm{e}}(t_{\mathrm{i}}) = -0.0854$ and $\dot{y}_{\mathrm{e}}(t_{\mathrm{i}}) = 0.0489$ m/s. The motion of the floating object and the FFSM are shown in Fig. 18. The impact impulse was computed as $I_{\mathrm{e,n}} = -0.4168$ Ns which resulted in

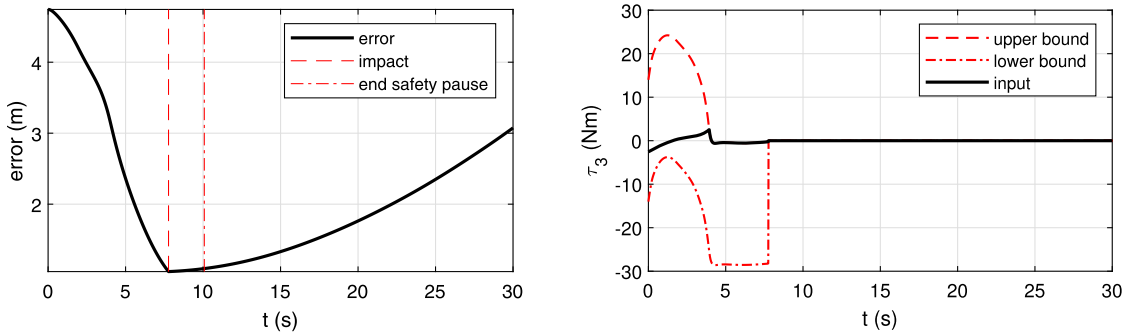

(a) The error. (b) The input.

Fig. 12. (a) The error of the gripper of FFSM. (b) The input torque of the third link without control.

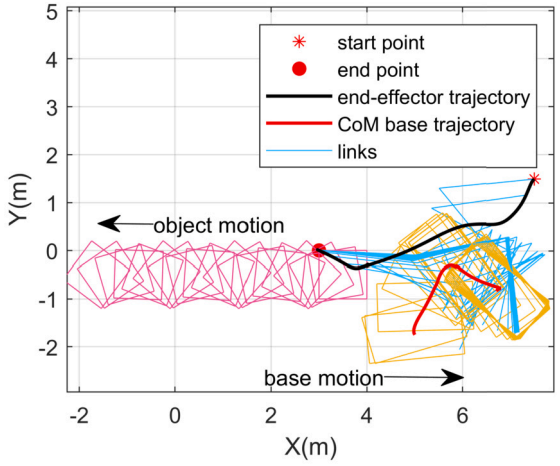

Fig. 13. The robot motion for free-flying case study. The ***video presentation*** of the simulation is available as the supplementary material of the paper.

the angular impulse of −0.0251 Nms. Thus, the object responded with a motion to the left and a clockwise rotation. The momentum of the FFSM is also illustrated in Fig. 19.

5. Conclusions

5.1. Concluding remarks

Although impact modeling between a robot end-effector and environment has been studied extensively in robotics, modeling of a free-floating space manipulator undergoing a collision with a floating object is still a challenging problem. In this paper, we present a complete solution to this problem, albeit under the simplifying assumptions of frictionless elastic impact, by using conservation of momentum and conservation of energy equations over the impact. Moreover, we solve this problem in the context of end-effector regulation control as the FFSM executes a point-to-point motion task while colliding with a floating object along the way. The controller of the FFSM is based on the output- and state-dependent Riccati equation approach which attempts to regulate the end-effector position, regardless of the free-floating condition of the carrier. The basis of this work is on free-floating dynamics of the FFSM. The base of the FFSM is completely floated and it does not use thrusters or reaction wheels. The simulation results were provided for the mentioned scenario and showed the effectiveness of the proposed modeling in the computation of the reaction impact force, velocities after collision, and control of the system.

It was found that the FFSM will drift away after finishing the control task due to the generation of the momentum of the impact on the base and the links of the robot. The focus of this work was not to address the compensation of this generated momentum though a free-flying controller was done briefly to show that control in a steady state is feasible, Section 4.4, which suggests more investigation in the future studies.

5.2. Future studies: penetration, pushing, and passing through the object

The modeling, control, and simulation of this research include the dynamics, and computation of the impact force and velocity after the collision. It does not include contact modeling to avoid penetration in case of colliding again after the impact; i.e., consider a case in which the end-effector is about to collide with the object, and the last link is almost horizontal. Then with this configuration, if the gripper collides with the object and the velocity of the object is not more than the whole collective velocity of the FFSM, the end-effector might move faster than the object. Then the simulation will show a case of penetration of the end-effector inside the body of the object. In reality, in such a case, the gripper must push the object until the velocity of the floating object exceeds the collective speed of the FFSM's gripper. In summary, the configuration of the FFSM is important to present a perfect simulation. It must be noted that this does not imply a defect in the formulation. It simply says that penetration and pushing were not modeled in this work and could be followed in future studies.

Declaration of competing interest

There is not any conflict of interest reported by the authors.

Acknowledgements

None.

Appendix A

The velocity components of the FFSM after the impact for the simulation Section 4.2. The velocity vector of the FFSM as a function of impact force:

$$\dot{\mathbf{q}}_{\mathrm{b}}(t_{\mathrm{i}}^{+}) = \begin{bmatrix} 0.12 - 0.012 I_{\mathrm{e,n}} \\ -7.5 \times 10^{-3} I_{\mathrm{e,n}} - 0.073 \\ -0.031 I_{\mathrm{e,n}} - 0.012 \\ 0.013 - 1.4 \times 10^{-4} I_{\mathrm{e,n}} \\ -0.14 I_{\mathrm{e,n}} - 0.27 \\ 0.37 I_{\mathrm{e,n}} + 0.55 \end{bmatrix}. \tag{35}$$

Substituting (35) into the conservation of momentum and energy equations (17) and (18) results in:

$$\begin{bmatrix} I_{\mathrm{e,n}} - 5\dot{x}_{\mathrm{o}}(t_{\mathrm{i}}^{+}) \\ -5\dot{y}_{\mathrm{o}}(t_{\mathrm{i}}^{+}) \\ 0.32 I_{\mathrm{e,n}} - 0.83\dot{\psi}_{\mathrm{o}}(t_{\mathrm{i}}^{+}) - 2.5\dot{x}_{\mathrm{o}}(t_{\mathrm{i}}^{+}) - 18\dot{y}_{\mathrm{o}}(t_{\mathrm{i}}^{+}) \\ f(I_{\mathrm{e,n}}, \dot{x}_{\mathrm{o}}(t_{\mathrm{i}}^{+}), \dot{y}_{\mathrm{o}}(t_{\mathrm{i}}^{+}), \dot{\psi}_{\mathrm{o}}(t_{\mathrm{i}}^{+})) \end{bmatrix} = \mathbf{0}, \tag{36}$$

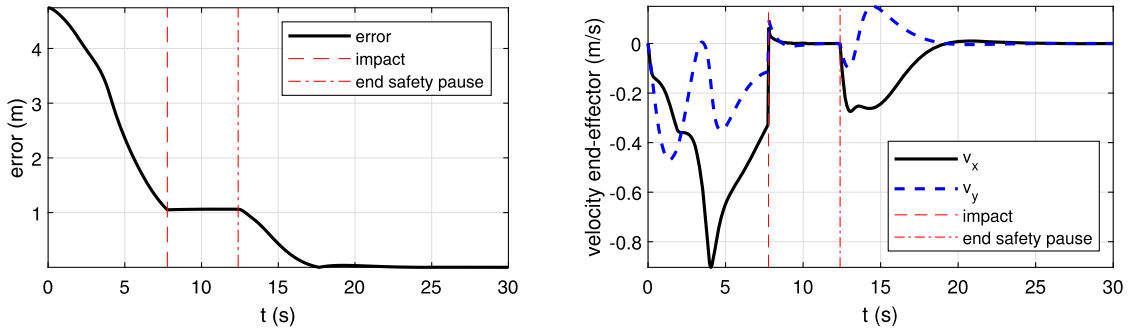

(a) The error. (b) The velocity.

Fig. 14. (a) The gripper error in free-flying simulation. (b) The velocity of the gripper for the free-flying robot.

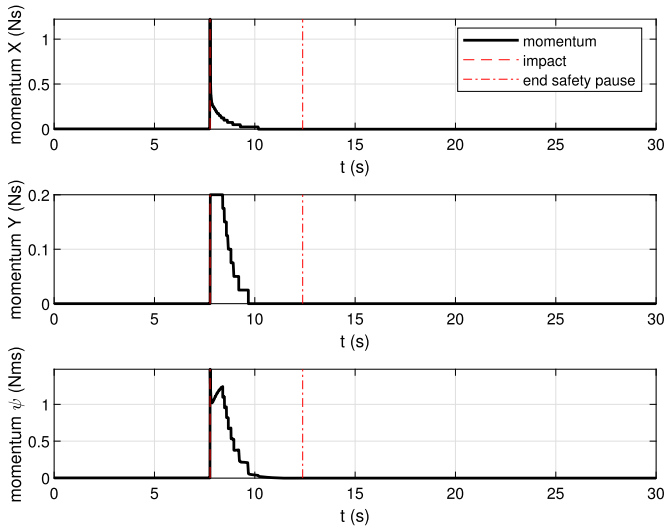

Fig. 15. The robot's momentum in the free-flying example. Please note that the pre-impact and resolution of the impact is similar to Section 4.2 and the jump of momentum after the impact is due to the actuation of the thrusters and motors of the FFSM.

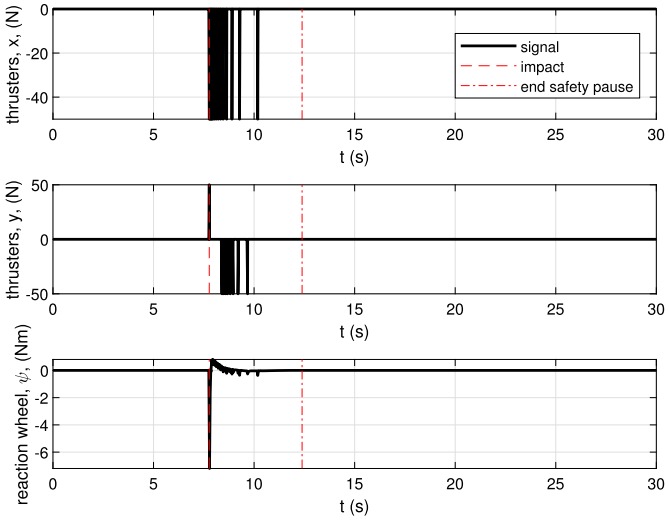

Fig. 16. The thrusters and reaction wheel inputs for the free-flying robot.

where

$$f(I_{e,n},\dot{x}_o(t_i^+),\dot{y}_o(t_i^+),\dot{\psi}_o(t_i^+)) = 0.33(0.17I_{e,n}+0.27)^2+0.5(0.29I_{e,n}+0.32)^2+(0.04I_{e,n}+0.076)^2+(0.031I_{e,n}+0.012)^2+(0.045I_{e,n}+0.15)^2+(0.085I_{e,n}+0.17)^2+0.33(0.2I_{e,n}+0.28)^2+0.5(0.14I_{e,n}+0.11)^2+2.5(7.5\times10^{-3}I_{e,n}+0.073)^2+(0.022I_{e,n}-0.11)^2+2.5(0.012I_{e,n}-0.12)^2+(0.22I_{e,n}+0.23)^2+0.42\dot{\psi}_o^2(t_i^+)+2.5\dot{x}_o^2(t_i^+)+2.5\dot{y}_o^2(t_i^+)+(0.08I_{e,n}+0.017)^2+0.33(0.032I_{e,n}-6.7\times10^{-4})^2-0.28,$$

is the result of the energy conservation equation. Solving (36) generates the unknown variables of the impact (force and velocities of the object after the impact):

$$\begin{bmatrix} I_{e,n} \\ \dot{x}_o(t_i^+) \\ \dot{y}_o(t_i^+) \\ \dot{\psi}_o(t_i^+) \end{bmatrix} = \begin{bmatrix} -1.2226 \\ -0.2445 \\ 0 \\ 0.2682 \end{bmatrix},$$

and substituting $I_{e,n}$ into (35) provides the velocity of the base and the links of the FFSM

$$\dot{\mathbf{q}}_b(t_i^+) = [0.1354, -0.0641, 0.0258, 0.0133, -0.1059, 0.0979]^\top.$$

Appendix B. Supplementary material

Supplementary material related to this article can be found online at https://doi.org/10.1016/j.ast.2024.108945.

References

[1] D.E. Hastings, C. Joppin, On-orbit upgrade and repair: the Hubble space telescope example, J. Spacecr. Rockets 43 (3) (2006) 614–625.
[2] M. Olivares-Mendez, M.R. Makhdoomi, B.C. Yalçın, Z. Bokal, V. Muralidharan, M.O. Del Castillo, V. Gaudilliere, L. Pauly, O. Borgue, M. Alandihallaj, et al., Zero-g lab: a multi-purpose facility for emulating space operations, J. Space Saf. Eng. (2023).
[3] Z.N. Khutorovsky, V.F. Boikov, L.N. Pylaev, Catalog maintenance of low-Earth-orbit satellites: principles of the algorithm, J. Guid. Control Dyn. 22 (6) (1999) 745–758.
[4] X. Zhao, W. Li, C. Zhao, J. Wang, Y. Cao, D. Du, Overall design of remote sensing large-platform satellite for on orbit assembly and maintenance, in: Ninth Symposium on Novel Photoelectronic Detection Technology and Applications, vol. 12617, SPIE, 2023, pp. 594–600.
[5] A. Rossi, L. Anselmo, C. Pardini, P. Farinella, A. Cordelli, Interaction of the satellite constellations with the low Earth orbit debris environment, in: Mission Design & Implementation of Satellite Constellations: Proceedings of an International Workshop, Toulouse, France, November 1997, Springer, France, 1998, pp. 327–335.
[6] C. Agabiti, E. Ménager, E. Falotico, Whole-arm grasping strategy for soft arms to capture space debris, in: 2023 IEEE International Conference on Soft Robotics (RoboSoft), IEEE, 2023, pp. 1–6.
[7] W. Lei, T. Zhao, G. Sun, Image based target capture of free floating space manipulator under unknown dynamics, Adv. Space Res. (2023).
[8] B. Dou, X. Yue, Disturbance observer-based fractional-order sliding mode control for free-floating space manipulator with disturbance, Aerosp. Sci. Technol. 132 (2023) 108061.

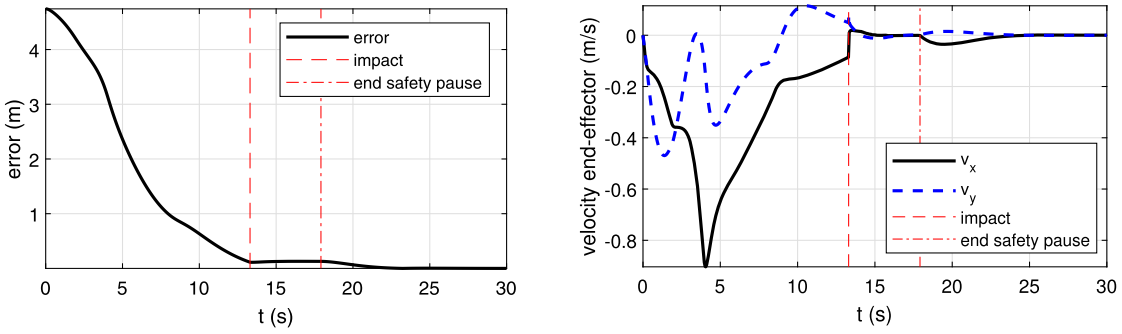

(a) The error. (b) The velocity.

Fig. 17. (a) The gripper error in regulation when the object is close to the endpoint. (b) The velocity of the gripper for this case.

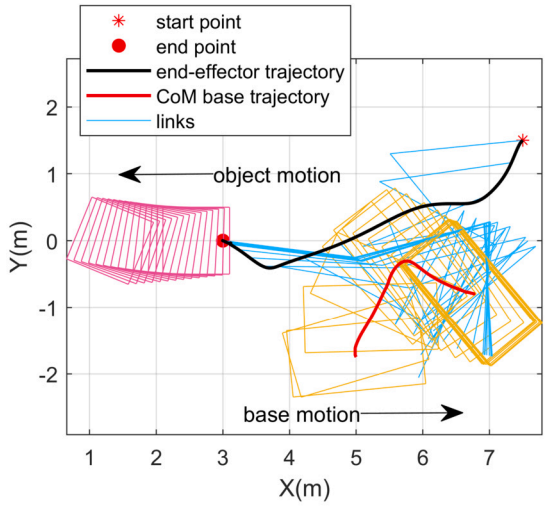

Fig. 18. The robot motion control and impact illustration when the object is close to the final point. The ***video presentation*** of the reaction and the impact is illustrated as the supplementary material of the paper.

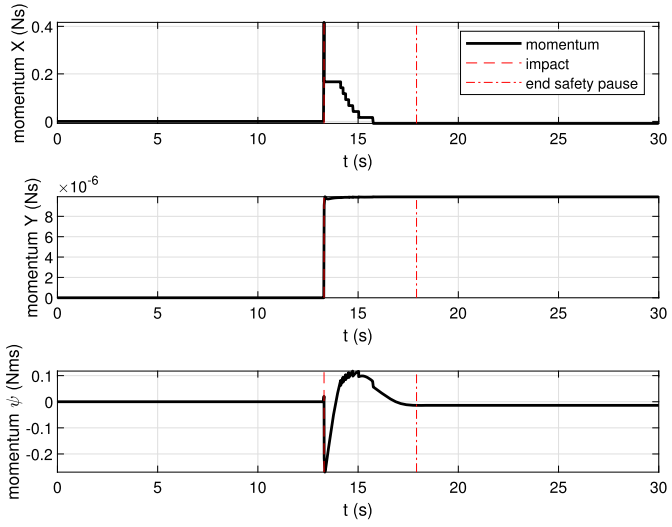

Fig. 19. The momentum of the space robot in slow impact simulation. The momentum reduction is through discontinuous steps since the thrusters are modeled by on-off actuators.

[9] G. Gilardi, I. Sharf, Literature survey of contact dynamics modelling, Mech. Mach. Theory 37 (10) (2002) 1213–1239.

[10] R. Featherstone, Rigid Body Dynamics Algorithms, Springer, 2014.

[11] S. Andrews, K. Erleben, Z. Ferguson, Contact and friction simulation for computer graphics, in: ACM SIGGRAPH 2022 Courses, ACM Digital Library, 2022, pp. 1–172.

[12] H. Asada, K. Ogawa, On the dynamic analysis of a manipulator and its end effector interacting with the environment, in: Proceedings. 1987 IEEE International Conference on Robotics and Automation, vol. 4, IEEE, 1987, pp. 751–756.

[13] K.P. Jankowski, H.A. El Maraghy, Dynamic decoupling for hybrid control of rigid-/flexible-joint robots interacting with the environment, IEEE Trans. Robot. Autom. 8 (5) (1992) 519–534.

[14] I. Rhee, G. Kang, S.J. Moon, Y.S. Choi, H.R. Choi, Hybrid impedance and admittance control of robot manipulator with unknown environment, Intell. Serv. Robot. 16 (1) (2023) 49–60.

[15] S. Jung, Sliding mode control for a hybrid force control scheme of a robot manipulator under uncertain dynamics, Int. J. Control. Autom. Syst. 21 (5) (2023) 1634–1643.

[16] X. Cyril, G.J. Jaar, A.K. Misra, The effect of payload impact on the dynamics of a space robot, in: Proceedings of 1993 IEEE/RSJ International Conference on Intelligent Robots and Systems (IROS'93), vol. 3, IEEE, 1993, pp. 2070–2075.

[17] D.N. Dimitrov, K. Yoshida, Momentum distribution in a space manipulator for facilitating the post-impact control, in: 2004 IEEE/RSJ International Conference on Intelligent Robots and Systems (IROS) (IEEE Cat. No. 04CH37566), vol. 4, IEEE, 2004, pp. 3345–3350.

[18] K. Nagaoka, R. Kameoka, K. Yoshida, Repeated impact-based capture of a spinning object by a dual-arm space robot, Front. Robot. AI 5 (2018) 115.

[19] J. Liu, Y. Tong, Y. Liu, Y. Liu, Development of a novel end-effector for an on-orbit robotic refueling mission, IEEE Access 8 (2020) 17762–17778.

[20] D. Raina, S. Gora, D. Maheshwari, S.V. Shah, Impact modeling and reactionless control for post-capturing and maneuvering of orbiting objects using a multi-arm space robot, Acta Astronaut. 182 (2021) 21–36.

[21] M. Ahmadizadeh, A. Shafei, R. Jafari, Frictional impact-contacts in multiple flexible links, Int. J. Struct. Stab. Dyn. 21 (06) (2021) 2150075.

[22] A. Shafei, H. Shafei, Oblique impact of multi-flexible-link systems, J. Vib. Control 24 (5) (2018) 904–923.

[23] R. Nekomoto, A. Sekiguchi, Dynamics simulation of biped robot with arch structure and toe joint, J. Adv. Comput. Intell. Intell. Inform. 27 (3) (2023) 404–410.

[24] Z. Liu, J. Gao, X. Rao, S. Ding, D. Liu, Complex dynamics of the passive biped robot with flat feet: gait bifurcation, intermittency and crisis, Mech. Mach. Theory 191 (2024) 105500.

[25] N. Memar Kocheh Bagh, P. Liu, Control and gait generation of biped robots: a review, in: The 1st International Conference on Intelligent Manufacturing and Robotics 2023 (ICiMR 2023), York, 2023, pp. 1–12.

[26] E.R. Westervelt, J.W. Grizzle, C. Chevallereau, J.H. Choi, B. Morris, Feedback Control of Dynamic Bipedal Robot Locomotion, CRC Press, 2018.

[27] Y. Xie, C. Gao, S. Zhu, X. Yan, L. Kong, A. Xie, J. Gu, D. Zhang, Gait optimization and energy-based stability for biped locomotion using large-scale programming, Robotica (2023) 1–21.

[28] E. Dantec, M. Naveau, P. Fernbach, N. Villa, G. Saurel, O. Stasse, M. Taix, N. Mansard, Whole-body model predictive control for biped locomotion on a torque-controlled humanoid robot, in: 2022 IEEE-RAS 21st International Conference on Humanoid Robots (Humanoids), IEEE, 2022, pp. 638–644.

[29] J.R. Guadarrama-Olvera, S. Kajita, G. Cheng, Preemptive foot compliance to lower impact during biped robot walking over unknown terrain, IEEE Robot. Autom. Lett. 7 (3) (2022) 8006–8011.

[30] B. Li, X. Gao, H. Huang, H. Yang, Nonlinear trajectory tracking control of underactuated auvs using the state-dependent Riccati equation (SDRE) with parameter perturbation, Nonlinear Dyn. 111 (19) (2023) 18027–18041.

[31] T. Çimen, State-dependent Riccati equation (SDRE) control: a survey, IFAC Proc. Vol. 41 (2) (2008) 3761–3775.

[32] S.R. Nekoo, Tutorial and review on the state-dependent Riccati equation, J. Appl. Nonlinear Dyn. 8 (2) (2019) 109–166.
[33] D.K. Parrish, D.B. Ridgely, Attitude control of a satellite using the SDRE method, in: Proceedings of the 1997 American Control Conference (Cat. No. 97CH36041), vol. 2, IEEE, 1997, pp. 942–946.
[34] P. Razzaghi, E. Al Khatib, S. Bakhtiari, Sliding mode and SDRE control laws on a tethered satellite system to de-orbit space debris, Adv. Space Res. 64 (1) (2019) 18–27.
[35] K. Sugiura, Y. Takao, A.K. Sugihara, Y. Sugawara, O. Mori, Formation flying along artificial halo orbit around Sun–Earth L2 point for interferometric observations, Acta Astronaut. 208 (2023) 36–48.
[36] D.-R. Lee, H. Pernicka, Optimal control for proximity operations and docking, Int. J. Aeronaut. Space Sci. 11 (3) (2010) 206–220.
[37] A.G. Romero, L.C. de Souza, State-dependent Riccati equation controller using Java in remote sensing CubeSats, J. Appl. Remote Sens. 13 (3) (2019) 032509.
[38] P. Huang, M. Wang, Z. Meng, F. Zhang, Z. Liu, Attitude takeover control for post-capture of target spacecraft using space robot, Aerosp. Sci. Technol. 51 (2016) 171–180.
[39] G. Sharma, B. Rout, Energy efficient reactionless design of multi-arm space robot for a cooperative handshake maneuver, Adv. Space Res. 71 (3) (2023) 1752–1768.
[40] S.R. Nekoo, Model reference adaptive state-dependent Riccati equation control of nonlinear uncertain systems: regulation and tracking of free-floating space manipulators, Aerosp. Sci. Technol. 84 (2019) 348–360.
[41] Q. An, Y. Zhang, Q. Hu, M. Li, J. Li, A. Mao, Time-optimal path tracking for dual-arm free-floating space manipulator system using convex programming, IEEE Trans. Aerosp. Electron. Syst. (2023).
[42] S.R. Nekoo, Output- and state-dependent Riccati equation: an output feedback controller design, Aerosp. Sci. Technol. 126 (2022) 107649.
[43] L. Roveda, D. Riva, G. Bucca, D. Piga, Sensorless optimal switching impact/force controller, IEEE Access 9 (2021) 158167–158184.
[44] O. Khatib, The potential field approach and operational space formulation in robot control, in: Adaptive and Learning Systems: Theory and Applications, Springer, 1986, pp. 367–377.
[45] Z. Zhu, Y. Yin, H. Lyu, Automatic collision avoidance algorithm based on route-plan-guided artificial potential field method, Ocean Eng. 271 (2023) 113737.
[46] W. Liu, K. Qiu, X. Yang, R. Wang, Z. Xiang, Y. Wang, W. Xu, Colregs-based collision avoidance algorithm for unmanned surface vehicles using modified artificial potential fields, Phys. Commun. 57 (2023) 101980.
[47] S.R. Nekoo, Nonlinear closed loop optimal control: a modified state-dependent Riccati equation, ISA Trans. 52 (2) (2013) 285–290.
[48] M. Asgari, H.N. Foghahayee, State dependent Riccati equation (SDRE) controller design for moving obstacle avoidance in mobile robot, SN Appl. Sci. 2 (11) (2020) 1928.
[49] M. Alirezaei, S. Jansen, J. Janssen, Experimental Evaluation of Collision Avoidance System Using State Dependent Riccati Equation Technique, CRC Press, 2015.
[50] Y. Xie, Z. Zhang, X. Wu, Z. Shi, Y. Chen, B. Wu, K.A. Mantey, Obstacle avoidance and path planning for multi-joint manipulator in a space robot, IEEE Access 8 (2019) 3511–3526.
[51] G.G. d. Castro, G.S. Berger, A. Cantieri, M. Teixeira, J. Lima, A.I. Pereira, M.F. Pinto, Adaptive path planning for fusing rapidly exploring random trees and deep reinforcement learning in an agriculture dynamic environment UAVs, Agriculture 13 (2) (2023) 354.
[52] W.F. Trench, Introduction to Real Analysis, Pearson College Div, 2002.
[53] Y. Hurmuzlu, D.B. Marghitu, Rigid body collisions of planar kinematic chains with multiple contact points, Int. J. Robot. Res. 13 (1) (1994) 82–92.
[54] A. Drouin, S.S. Cunha, A.C.B. Ramos, F. Mora-Camino, Differential flatness and control of nonlinear systems, in: Proceedings of the 30th Chinese Control Conference, IEEE, 2011, pp. 643–648.
[55] M.H. Korayem, S.R. Nekoo, Controller design of cooperative manipulators using state-dependent Riccati equation, Robotica 36 (4) (2018) 484–515.
[56] H. Banks, B. Lewis, H.T. Tran, Nonlinear feedback controllers and compensators: a state-dependent Riccati equation approach, Comput. Optim. Appl. 37 (2007) 177–218.